Targeting the TREK-1 potassium channel via riluzole to eliminate the neuropathic and depressive-like effects of oxaliplatin

Laura Poupon, Sylvain Lamoine, Vanessa Pereira, David Barriere, Stéphane Lolignier, Fabrice Giraudet, Youssef Aissouni, Mathieu Meleine, Laetitia Prival, Damien Richard Richard, et al.

Research Article:

Title: Targeting the TREK-1 potassium channel via riluzole to eliminate the neuropathic and depressive-like effects of oxaliplatin

Authors: Laura POUPON[1*], Sylvain LAMOINE[1*], Vanessa PEREIRA[1], David A. BARRIERE[1], Stéphane LOLIGNIER[1], Fabrice GIRAUDET[1], Youssef AISSOUNI[1], Mathieu MELEINE[1], Laëtitia PRIVAL[1], Damien RICHARD[1], Nicolas KERCKHOVE[1,2], Nicolas AUTHIER[1,2], David BALAYSSAC[1,2], Alain ESCHALIER[1,2§], Michel LAZDUNSKI[3,4§], Jérôme BUSSEROLLES[1,2§].

Affiliations:

[1] *Université Clermont Auvergne, Inserm, CHU Clermont-Ferrand, Neuro-Dol, F63000, Clermont-Ferrand, France*

[2] *Institut Analgesia, Faculté de Médecine, BP38, 63001, Clermont-Ferrand, France*

[3] Université de Nice Sophia Antipolis, 06560 Valbonne, France

[4] CNRS, Institut de Pharmacologie Moléculaire et Cellulaire, UMR 7275, 660 Route des Lucioles Sophia Antipolis, 06560 Valbonne, France.

*These authors contributed equally to the work

Number of text pages of the entire manuscript: 26

Number of figures: 7

(§) Correspondence:

Pr Eschalier, Université Clermont Auvergne, Inserm, CHU Clermont-Ferrand, Neuro-Dol, F63000, Clermont-Ferrand, France

email : alain.eschalier@uca.fr ; tel 33(0) 4 73 17 82 30 ; fax 33(0) 4 73 27 71 62

Pr Lazdunski, CNRS, IPMC, UMR 7275, 660 Route des Lucioles Sophia Antipolis, 06560 Valbonne, France

email : lazdunski@ipmc.cnrs.fr ; tel 33(0) 4 93 95 77 03; fax 33(0) 4 93 95 77 04

Dr Busserolles, Inserm, U1107, Neuro-Dol, Faculty of Medicine, 28, pl. H.Dunant, 63000 Clermont-Ferrand, France

email :jerome.busserolles@uca.fr ; tel 33(0) 4 73 17 82 35 fax 33(0) 4 73 27 71 62

The authors have declared that no conflict of interest exists.

Abstract:

Neurotoxicity remains the most common adverse effect of oxaliplatin, limiting its clinical use. In the present study, we developed a mouse model of chronic oxaliplatin-induced neuropathy, which mimics both sensory and motor deficits observed in patients, in a clinically relevant time course. Repeated oxaliplatin administration in mice induced both cephalic and extracephalic long lasting mechanical and cold hypersensitivity after the first injection as well as delayed sensorimotor deficits and a depression-like phenotype. Using this model, we report that riluzole prevents both sensory and motor deficits induced by oxaliplatin as well as the depression-like phenotype induced by cumulative chemotherapeutic drug doses. All the beneficial effects are due to riluzole action on the TREK-1 potassium channel, which plays a central role in its therapeutic action. Riluzole has no negative effect on oxaliplatin antiproliferative capacity in human colorectal cancer cells and on its anticancer effect in a mouse model of colorectal cancer. Moreover, riluzole decreases human colorectal cancer cell line viability in vitro and inhibits polyp development in vivo. The present data in mice may support the need to clinically test riluzole in oxaliplatin-treated cancer patients and state for the important role of the TREK-1 channel in pain perception.

Keywords: oxaliplatin, TREK-1 potassium channel, riluzole, neurotoxicity, prevention, colorectal cancer

1. Introduction

The anticancer agent oxaliplatin (Andre et al., 2004), has neuropathic effects that can limit its clinical use (Beijers et al., 2015; Pachman et al., 2015). More than 90% of patients experience acute pain symptoms that are induced or exacerbated by cold and localized to the extremities and the face in hours or days following oxaliplatin infusions. Those symptoms do not always completely resolve between treatment cycles (Pachman et al., 2015) and 30-50% of patients suffer from chronic oxaliplatin-induced peripheral neuropathy (OIPN) (Beijers et al., 2015). This cumulative and dose-dependent sensory neuropathy (Grothey, 2005) leads to a limit in dosage or changes in treatment to less neurotoxic agents with the risk of reducing the effective clinical outcome (Hartmann and Lipp, 2003), and may be accompanied by comorbidities such as distress, depression and anxiety (Tofthagen et al., 2013). Currently, none of the drugs used for prevention or treatment of OIPN have been shown to be sufficiently effective to be incorporated routinely into clinical practice (Hershman et al., 2014).

Peripheral sensory neurons damage (Binder et al., 2007; Cavaletti et al., 2001; Di Cesare Mannelli et al., 2013; Renn et al., 2011) and function alterations (Park et al., 2009a; Park et al., 2009b; Renn et al., 2011) seem to play an important role in OIPN development. Notably, oxaliplatin has been proposed to be a channelopathy inducer (Descoeur et al., 2011; Grolleau et al., 2001). Our group has shown that oxaliplatin treatment leads to a drastic down-modulation of TREK-1 and TRAAK potassium channels in nociceptors (Descoeur et al., 2011), two members of the K2P channels family (Bayliss and Barrett, 2008; Brohawn et al., 2014; Dong et al., 2015; Enyedi and Czirjak, 2010; Lesage, 2003; Lesage and Lazdunski, 2000; Lesage et al., 2000; Maingret et al., 1999a; Maingret et al., 2000; Mathie and Veale, 2007; Patel et al., 1998) involved in polymodal pain perception (Alloui et al., 2006; Noel et al., 2009). Mice lacking the TREK-1 and TRAAK channels have an increased sensory perception that resembles those observed in wild-type mice treated with oxaliplatin, and oxaliplatin fails to change significantly cold and mechanical perception in these double KO mice (Descoeur et al., 2011).

Oxaliplatin also leads to a massive increase of glutamate in the cerebrospinal fluid (Yamamoto et al., 2017). This is similar to the synaptic increase of glutamate that is known to occur in brain, spinal cord or retinal ischemia and that is found to be very deleterious for the neuronal cells (Benveniste et al., 1984; Choi and Rothman, 1990; Louzada-Junior et al., 1992; Nishizawa, 2001; Simpson et al., 1990).

Riluzole, an oral drug used for the treatment of amyotrophic lateral sclerosis (ALS) (Lacomblez et al., 1996) is an activator of TREK-1 and TRAAK channels (Duprat et al., 2000) and also of TREK-2, a close member also involved in pain perception (Pereira et al., 2014). We then reasoned that an activator of K^+ channels of the TREK-1 family, such as riluzole, could reverse the negative effects of oxaliplatin by boosting the K^+ channel activity of the small proportion of the remaining channels to restore, at least partly, the original activity. In addition, riluzole is a blocker of excessive glutamate accumulation in oxaliplatin treated animals as it is in ischemic animals (Heurteaux et al., 2006a; Lang-Lazdunski et al., 1999; Wu et al., 2014; Yamamoto et al., 2017). This effect is known to provide a preservation of neuronal structures in brain, spinal cord and retinal ischemia (Ettaiche et al., 1999; Heurteaux et al., 2006a; Lang-Lazdunski et al., 2000). Here again, there is a good probability that this glutamate effect of riluzole is due to its capacity to activate TREK channels which are known to be central K^+ channels in neuroprotection (Heurteaux et al., 2004; Wu et al., 2013).

This paper extents our earlier observation that riluzole indeed antagonizes the deleterious effect of oxaliplatin (Busserolles, 2010). Hence, the data that are presented here converge to show that riluzole can counteract the sensory, motor and affective adverse effects induced by oxaliplatin treatment. This paper also reports that riluzole does not negatively affect oxaliplatin anti-tumoral effect *in vitro* or *in vivo*.

2. Materials and Methods

2.1. Animals

All experiments were performed on 20–24 g male mice (total number of mice: 565). C57Bl/6JRj mice were purchased from Janvier Labs (Le Genest St Isles, France). All transgenic animals were mice of the N10F2 backcross generation to C57Bl/6J inbred congenic strain. The detailed experimental methodology used to generate and genotype (done by cutting ear tip) TREK-1, TREK-2 and TRAAK knock-out mice and their respective wild-type littermates has been previously described (Heurteaux et al., 2004). Triple KO mice were generated by crossing TREK1$^{-/-}$-TREK2$^{-/-}$ and TREK1$^{-/-}$-TRAAK$^{-/-}$ mice, resulting in TREK1$^{+/-}$-TREK2$^{+/-}$-TRAAK$^{+/-}$ offsprings. Triple knockout mice were obtained by intercrossing this progeny. C57BL/6J-Apc$^{Min/+}$ mice (*Apc$^{Min/+}$* mice; The Jackson Laboratory) are a gift from Dr. Mathilde Bonnet (UMR Inserm U1071, Clermont-Ferrand, FRANCE). All mice were grouped housed in a temperature-controlled environment with food and water *ad libitum*. The behavioural experiments were performed blind to the genotype and/or treatment, with randomization of treatments, in a quiet room, by the same experimenter for a given test taking great care to avoid or minimize discomfort of the animals. Treatment administrations were performed according to the method of equal blocks, to assess the effect of the different treatments at the same time interval so as to avoid unverifiable and time-variable environmental influences. All animal procedures were approved by the local Animal Ethics Committee and experiments were performed according to both the ARRIVE guidelines and the guidelines provided by the European Community guiding in the care and use of animals (Directive 2010/63/EU).

2.2. Drugs administration and experimental design

The following drugs were used: oxaliplatin (Sanofi Aventis, France), riluzole (Abcam), the TREK-1 blocker spadin (kind gift from Dr Marc Borsotto, IPMC, Nice, France), the antineoplasic agent 5-fluorouracil (5-FU) (Accord Healthcare France). All solutions were prepared just before experiments in 0.9% (w/v) NaCl solution for spadin and riluzole (only for injections in acute model), in a 5% glucose solution for oxaliplatin and in the drinking water for riluzole (in chronic model).

For the chronic administration, we have chosen to administrate riluzole in the drinking water rather than by oral drug delivery gavage in order to minimize the stress associated with repeated gavage or daily injections. We administered a 60 µg/mL concentration of riluzole, as described previously (Gurney et al., 1996), translating to 13.2 mg/kg/day. We measured twice a week the water consumption of C57Bl/6JRj mice treated or not with oxaliplatin and riluzole (n = 5 per group) by weighting their baby bottles. The mean water consumption for the study was not significantly different between the groups (2.98 +/- 0.27 mL/mouse for the vehicle group, 2.89 +/- 0.09 mL/mouse for the riluzole group, 3.00 +/- 0.14 mL/mouse for the oxaliplatin group and 2.92 +/- 0.16 mL/mouse for the riluzole + oxaliplatin group). We additionally measured blood riluzole concentration in mice from experiment 2 (see below) receiving or not riluzole in the drinking water using Liquid chromatography and mass spectrometry. 20µL of standard, control or sample preparation were injected into liquid chromatography systems (transcend TLX II, Thermo Fisher, San Jose, USA). On-line chromatography purification was caring using turbulent flow column (cyclone P 0.5 x 50 mm) at 1.5mL/min between 30s. Elution step used 200µL of acetonitrile/water (0.1% formic acid) (40/60; v/v). Chromatographic separation was carried out using a reverse-phase liquid at 30°C using a Hypersil GOLD Pentafluorophenyl column (50 x 2.1 mm, 1.9µm) (Thermo Fisher Scientific, San Jose, CA, USA). Analytical step used gradient system with the mobile phase consisting of solvent A (0.1%; v/v; formic acid in water) and solvent B (0.1%; v/v; formic acid in acetonitrile) at a flow rate of 400µL/min. Run time was set to 12.57min. The auto sampler was kept at 8°C.

The MS analysis was performed using a Thermo Q-Exactive Plus benchtop Orbitrap® instrument. We used a heated electrospray ionization source (HESI II). The compounds were ionized by the source in positive mode. Acquisition was in SIM (Single Ion Monitoring) with selected molecular ions m/z 141.14305 for IS and m/z 235.01414 for riluzole at a resolution of 70,000 (FWHM). A second event was use for full fragmentation at 30 eV, at a resolution of 17,500 (FWHM), for IS and riluzole specifically. The concentration of riluzole were determined by their area ratios to that of the IS using a weight quadratic fit. Confirmation ion used one fragmentation ion for IS (m/z

93.06700) and riluzole (m/z 166.01920). Lower limit of quantification (LLOQ) of riluzole was 5 µg/L and upper limit of quantification (ULOQ) was 2500 µg/L in plasma.

Oxaliplatin-induced acute neuropathy: TREK-1, TREK-2 and TRAAK knock-out mice and their respective wild-type littermates were injected once intraperitoneally with oxaliplatin at 6 mg/kg. Cold-sensitivity was assessed using the tail immersion test (10°C) prior and 96h after drug administration. 96h corresponds to the peak of oxaliplatin related cold-hyperalgesia (Descoeur et al., 2011). The same protocol has been used in C57Bl/6JRj mice in which spadin (1 mg/kg, s.c.) or its vehicle was injected 30 minutes prior to riluzole (7.5mg/kg, i.p.).

Oxaliplatin-induced chronic neuropathy: TREK-$1^{+/+}$ and TREK-$1^{-/-}$ mice were injected twice a week for 4 weeks intraperitoneally with oxaliplatin at 6 mg/kg with or without riluzole treatment (60 µg/mL in the drinking water). Cold sensitivity was evaluated before and once a week after the first oxaliplatin administration in both extracephalic and cephalic areas using the tail immersion test (10°) and the acetone test respectively. Mechanical sensitivity at both extracephalic and cephalic levels was also evaluated using the von Frey and brush tests respectively with a similar time course after oxaliplatin treatment. The beam walk and adhesive removal tests were used at day 7 and at day 28. The forced swimming test and the novelty suppressed feeding test were used at day 28. All the tests were performed before oxaliplatin administrations. Body weight and body temperature, monitored with a rectal probe (Microprobe Thermometer, BAT-12, WPI, Sarasota, USA), as well as circulating riluzole concentration were monitored in some of non-knock-out animals. We performed four independent experiments in both TREK-$1^{+/+}$ and TREK-$1^{-/-}$ mice. In the first one (experiment 1) two blocks of TREK-$1^{+/+}$ and TREK-$1^{-/-}$ mice were subjected to the tail immersion test and the brush test once a week, and to the forced swimming test at day 28. In the second one (experiment 2) two blocks of TREK-$1^{+/+}$ and TREK-$1^{-/-}$ mice were subjected to the von Frey test and the acetone test once a week. In the third one (experiment 3) two blocks of TREK-$1^{+/+}$ and TREK-$1^{-/-}$ mice were subjected to the beam walk and the adhesive removal test at day 7 and at day 28. In the fourth one (experiment 4) two blocks of TREK-$1^{+/+}$ and TREK-$1^{-/-}$ mice were subjected to the novelty suppressed feeding test at day 28. Two independent experiments

(experiments 5 & 6) were also carried out in C57Bl/6JRj mice to measure caudal nerve conduction velocity. Morphological analysis of dorsal root ganglion neurons and of sciatic nerve mitochondria was made on tissues obtained from these experiments. Two independent experiments have been performed in $APC^{Min/+}$ mice. In the first one (experiment 7) animals were subjected to both the tail immersion and acetone tests, and at day 28 small intestine and colon were removed to quantify polyps number and tumor volume. In the second one (experiment 8), thermal cold pain symptoms were assessed using the tail immersion test once a week after the first injection of oxaliplatin (6 mg/kg, i.p.) with riluzole treatment (60 µg/mL in the drinking water). Spadin (1mg/kg, s.c.) was administered in one group of oxaliplatin and riluzole-treated mice 30 minutes before the test. Animal receiving neither oxaliplatin, nor riluzole or spadin served as control.

5FluoroUracil (5FU) + oxaliplatin-induced chronic neuropathy: Thermal cold pain symptom was assessed using the tail immersion test in mice co-administered with oxaliplatin (2 mg/kg) and 5-FU (15mg/k) by i.v. route twice a week for 4 weeks, with or without riluzole treatment (60 µg/mL in the drinking water) in C57Bl/6JRj mice.

2.3. Tail Immersion test.

Extra cephalic thermal nociceptive responsiveness was determined using the cold water (10°C) tail immersion test in mice briefly immobilized by gently wrapping them in a soft tissue. The lower 3 cm portion of the tail was immersed in a temperature-controlled water bath until withdrawal was observed (cutoff time, 30 seconds). The latency to the first rapid tail flick represented the behavioral endpoint (Janssen et al., 1963).

2.4. Von Frey test.

Extra cephalic mechanical pain hypersensitivity was assessed using a 0.6g bending force calibrated von Frey hair filament (Bioseb, France) that was pressed (during 2 seconds) perpendicularly to the plantar surface of the hind paw until it bent. Five stimuli were applied with an interval of 3–5 s and the number of responses measured.

2.5. Acetone Test.

Cephalic reflex responses to innocuous cool temperatures were assessed using the acetone test (Choi et al., 1994). Mice were placed in a plexiglas box (11.5 x 7.5 x 7 cm) for upper lip stimulation, and allowed to acclimate for 30 min. An acetone drop (20µL) was gently applied to the upper lip area skin surface and the total time spent in acetone-evoked behaviors (grooming, scratching and flinching) was counted over the next minute period. Acetone was applied 2 times (with a 5 min interval between successive applications), and the mean of the cumulated responses (total duration of nocifensive behaviors for the 2 successive applications) were calculated.

2.6. Brush Test.

Cephalic dynamic mechanical hypersensitivity was assessed using the brush test. Mice were placed in a plexiglas box (11.5 x 7.5 x 7 cm) for upper lip stimulation, and allowed to acclimate for 30 min. A "marten" brush was used to lightly stroke the upper lip area skin surface for 3 seconds. Five stimuli were applied with an interval of 3-5 seconds and the number of responses measured. The reaction of the animal consists of a decline or avoidance of the brush.

2.7. Beam Walk.

Gross vestibulomotor function was evaluated with the beam-balance task which involves placing the mice on a suspended (50cm from the floor) narrow wooden beam (5 mm diameter, 80 cm lenght). Performance on the beam was quantified by measuring the time needed by the mouse to cross the beam and the number of paw slips that occured in the process.

2.8. Adhesive Removal test.

This test was performed to assess sensorimotor deficits as previously described (Bouet et al., 2009). Briefly, one adhesive tape (0.3-0.4 cm) was attached on each mouse forepaw and the time to remove the tape was measured (cut off 300s).

2.9. Forced swimming test (FST).

FST was adapted from the traditional method that is described in a detailed reference (Porsolt et al., 1977). Briefly, mice were individually forced to swim in an open cylindrical container (diameter 14 cm, height 20 cm), containing 10 cm of water (depth) at (24 ± 1°C). Each animal was

forced to swim for six min, and the first immobilization and total duration of immobility were measured.

2.10. Novelty suppressed feeding (NSF) test.

The NSF test was performed according to the method described previously in a light intensity (35 lux) regulated room (Santarelli et al., 2003). Animals were food-deprived for 24 h prior to the test. A single weighed pellet of food was placed on a white circular filter paperplat-form positioned in the center of a clear plastic (40 × 40 × 20 cm) arena. Mice were tested individually after placing them in the corner of the box for 5 min. The latency to both detect and eat the pellet was manually scored.

2.11. Caudal nerve conduction velocity.

The measurement procedure was adapted from Petit et al. [45]. In all four mice groups, nerve conduction velocity (NCV) was measured the day prior to the initiation of the weekly treatment during four weeks. Mice were anesthetized with 1% iso-flurane (by inhalation, for induction and maintenance) (EZ-7000, EZ Anesthesia, WPI, Sarasota, USA) and placed in a prone position for recording. Body temperature was continuously monitored with a rectal probe (Microprobe Thermometer, BAT-12, WPI, Sarasota, USA) and strictly maintained constant at 37 °C with a thermostat-controlled heating pad (Homeothermic Blanket System, Harvard Apparatus, Holliston, USA). Caudal nerve conduction velocities were recorded by stimulating the caudal nerve using a Neuropack μMEB-9100 recording device (Nihon Koden, Tokyo,Japan) and needle electrodes (stainless steel, diameter: 0.4 mm, Medtronic Xomed Inc., Minneapolis, USA). At the base of the tail a pair of recording needle electrodes was placed, while a pair of stimulating needle electrodes was placed 60 mm caudally. Stimulating electrodes and recording electrodes were inserted in the tail 60mm apart. A ground needle electrode was inserted between the stimulating and recording. 20 stimuli with supramaximal stimulation intensity (intensity 1 mA, 0.1 ms duration, 3Hz frequency) were averaged to measure nerve conduction (high-pass filter: 2 Hz; low-pass filter: 5 kHz).

2.12. Morphological analysis of dorsal root ganglion neurons and sciatic nerves.

C57Bl/6JRj mice received oxaliplatin (6 mg/kg, i.p.) or vehicle (Glucose 5%) twice a week for 4 weeks with or without riluzole (60 µg/mL) in the drinking water from day 0 to 28. Three mice of each group were killed under pentobarbital (200 mg/kg, i.p.) anesthesia by perfusion through the left ventricle with 0.9% normal saline followed by freshly prepared 4% paraformaldehyde (PFA) and 2.5% glutaraldehyde in 0.1 M phosphate buffered saline (PBS), using a peristaltic pump (rate: 20 mL/min for 5 min). DRG neurons and sciatic nerves were removed and post-fixed overnight at 4 °C in the same fixative solution. To obtain semi-thin sections, DRG neurons were extensively washed with PHEM buffer and then post-fixed in 1% osmium tetroxide for 90 minutes at 4°C. Samples were then washed three times and kept in 70° ethanol overnight at 4°C. Sections were then dehydrated through a series of alcohols and acetone. Samples were embedded in epoxy resin with an automatic microwave tissue processor (Leica), and then semi-thin coronal sections (700 nm in thickness) were cut (ultramicrotome UC6, Leica) and stained with toluidine blue for examination under an optical microscope at 200× magnification. Ultrathin sections, 70 nm in thickness, were stained with uranyl acetate and lead citrate and specimens sections were observed at 80 kV with a Hitachi H-7650 TEM and a camera Hamamatsu AMT40. Mitochondrial morphological analysis was performed on ultrathin section of sciatic nerve at 8000x or 60000x magnification. Analysis was realized with ImageJ software and mitochondria were counted and classified regarding their normal, vacuolated or degraded morphology. The analysis was performed on three animals per groups and at least 200 mitochondria were counted for myelinated fibers and 50 mitochondria for unmyelinated fibers. Cellular dimensions of L4–L6 DRGs were measured using a method adapted from Tomiwa et al (1986) and Coggeshall et al (1990) and following previously established size criteria (Obata et al, 2003). In these sections, using a 200× oil immersion objective lens, the number of neurons with nuclei, nucleoli, multiple nucleoli, and nucleolar eccentricity was counted. Eccentricity of the nucleolus was identified when its center (or that of the largest one if there appeared to be more than one) lays in the outer half of the radius of the nucleus. The results were expressed as percentage of those cells with a visible nucleolus. At least 59 cells were analyzed per DRG.

2.13. Cell culture.

HT-29 (ATCC, HTB-38) and T84 (ATCC, CCL-248) human CRC cells were a kind gift from Dr M. Bonnet. Cells were cultured in Dulbecco's modified Eagle's medium (DMEM) for HT29 cells and in DMEM/F12 medium for T84 cells, at 37°C in a humidified atmosphere of 95% air/5% CO_2. All media were supplemented with 10 % $^{v}/_{v}$ heat-inactivated fetal bovine serum (FBS), 1% penicillin/streptomycin, 1% MEM vitamins, 1% pyruvate, 1% glutamine, 1% MEM non-essential amino acids. Drugs used were dissolved in 100% DMSO. The treatments were realized as the final concentration of DMSO not exceeding 0.4%.

2.14. Cell viability assay:

3-(4,5-Dimethylthiazol-2-yl)-2,5-diphenyltetrazolium bromide (MTT) assay was done according to the manufacturer's protocol (Life Technologies). Briefly, 7.5 10^3 cells were plated in a 96-well plate and treated for 48h with oxaliplatin and/or riluzole as indicated. Quantification of the MTT assays was performed using an Epoch microplate spectrophotometer (Biotek Instruments, Inc., Winooski, VT). The absorbance of vehicle treated cells (not exceeding 0.4% of DMSO) was designated as 100% and cell survival expressed as a percentage of this value. Data shown represent the mean ± SEM of three independent experiments performed in triplicate.

2.15. $APC^{Min/+}$ mice tumor analysis

$APC^{Min/+}$ mice were killed by cervical dislocation under anesthesia with iso-flurane (EZ-7000, EZ Anesthesia, WPI, Sarasota, USA). The entire gastrointestinal tract was immediately removed, washed with phosphate buffered saline (PBS), and divided into two segments: from proximal small intestine to distal small intestine (duodenum + jejunum), and colon. After identification of the specific intestinal regions, samples were bisected longitudinally and the number of polyps was recorded as well as their diameters measured with calipers by two independent investigators blinded to the results.

2.16. Statistics.

Data were analyzed using the Graphpad Prism software program Version 6.0. Statistical analysis was performed using a two-way repeated measure analysis of variance (RM ANOVA) for data of

the kinetics of painful scores and body weight and body temperature monitoring, followed by a Bonferroni post hoc test. A two-way analysis of variance (ANOVA) was used for data of the area under the curves (AUC) from Figure 1, for data from Figures 3-6, 7D-E, followed by a Bonferroni post hoc test. A one-way analysis of variance (ANOVA) was used for data from Suppl. data 3B and Suppl. data 3B. The specific tests used are indicated within the text of the figure legends, and power analysis for all the tests is provided as a Table 1.

3. Results

3.1. Riluzole exerts an analgesic effect in acutely oxaliplatin-treated animals that involves activation of the K_2P ion channel TREK-1

We assessed the analgesic effect of riluzole in a model of acute neuropathic pain induced by a single injection of oxaliplatin as previously described (Descoeur et al., 2011). Mice deleted for the TREK-1, TREK-2 or TRAAK channel encoding genes and their respective wild-type littermates were treated with either vehicle or riluzole (7.5 mg/kg, i.p.) 4 days after a single oxaliplatin injection (6 mg/kg, i.p.), corresponding to the peak of hypersensitivity previously reported in this model (Descoeur et al., 2011). Our previous work (Noel et al., 2009) has shown that the combined deletion of TREK-1 and TRAAK channels in mice led to increased cold sensitivity, and eliminated the ability of oxaliplatin to cause further cold hypersensitivity. The same observation was made for triple TREK-1/TREK-2/TRAAK knock-out animals (Pereira et al., 2014). However the sole deletion of TREK-1 (Alloui et al., 2006; Noel et al., 2009), is not sufficient to alter nociceptive cold sensitivity (**Suppl. data1**). Riluzole induced an analgesic effect in oxaliplatin-treated wild-type animals that was totally lost in *TREK1*$^{-/-}$ mice (**Fig. 1A, Table 1 N°1A kinetics & N°1A AUC**) but not in *TREK-2*$^{-/-}$ mice (**Fig. 1B, Table 1 N°1B kinetics & N°1B AUC)** or in *TRAAK*$^{-/-}$ mice (**Fig. 1C, Table 1 N°1C kinetics & N°1C AUC)**, suggesting a major and specific contribution of the TREK-1 channel in the analgesic effect. Consistent with this result, the pharmacological blockade of TREK-1 channel by spadin, a selective inhibitor of TREK-1 channel function that can both inhibit the channel activity of TREK-1 and trigger extensive internalization (Mazella et al., 2010), also led to

a loss of the analgesic effect of riluzole in this model **(Fig. 1D, Table 1 N°1D kinetics & N°1D AUC)**. Riluzole also has an antinociceptive effect to cold in naïve animals not treated by oxaliplatin that is lost in both TREK-1 and triple knock-out animals (**Suppl. Data 1, Table 1 N° Suppl. data 1**). We then decided to evaluate the neuroprotective effect of riluzole, and the TREK-1 channel involvement, in mice treated with repeated oxaliplatin injections.

3.2. Repeated oxaliplatin administration induces extracephalic and cephalic pain hypersensitivity that is prevented by riluzole treatment

Prolonged oxaliplatin treatment is known to induce a persistent sensory peripheral neuropathy that particularly affects extremities as well as the orofacial area. We evaluated the development of these symptoms in *TREK-1*$^{+/+}$ and *TREK-1*$^{-/-}$ mice administered with oxaliplatin (6 mg/kg, i.p.) twice a week for 4 weeks with or without riluzole administration in the drinking water (60 µg/mL p.o.) from day 0 to day 28 (**Fig. 2A**). We administered a 60 µg/ml concentration of riluzole (as previously described (Gurney et al., 1996)) translating to 13.2 mg/kg/day. This corresponds after correction for the body surface area (Reagan-Shaw et al., 2008) to a dose of 1.07 mg/kg/day in man, i.e. an administration of 85.6 mg/day for a man of 80 kg. ALS patients receive orally 100 mg of riluzole/day. The blood concentration of riluzole in mice (51.5 +/- 7.7 ng/mL; **Suppl. Data 2A**) is similar to the blood concentration of riluzole found in humans patients (median trough concentration : 54 ng/ml), who also take the drug orally (Groeneveld et al., 2008).

Oxaliplatin treatment slowed down the normal growth of animals. However, neither oxaliplatin nor riluzole led to significant animal weight loss (**Suppl. data 2B, Table 1 N° Suppl. data 2B**) or body temperature changes **(Suppl. data 2C, Table 1 N° Suppl. data 2C)** along the experiment. The cold hypersensitivity was established in oxaliplatin-treated mice from day 7 after the first injection in both extracephalic and cephalic areas as evidenced by the significant decrease in tail withdrawal latency in response to a noxious cold stimulation (10°C) **(Fig. 2B, Table 1 N° 2B)** and the increase of acetone-evoked behaviors (grooming, scratching and flinching) **(Fig. 2C, Table 1 N° 2C),** respectively. Mechanical hypersensitivity at both extracephalic (**Fig. 2D, Table 1 N° 2D)**

and cephalic levels **(Fig. 2E, Table 1 N° 2E)** was also observed with a similar time course after oxaliplatin treatment in oxaliplatin-treated animals. Daily riluzole administration (60 µg/mL, p.o) significantly prevented both cold and mechanical hypersensitivities induced by oxaliplatin in all tested areas (**Fig. 2 B, C, D, E)**. **Fig. 2 (F, G, H, I)** shows that, whatever the stimulus (mechanical or thermal) and the dermatomes tested (face or hindpaws), riluzole totally lost its analgesic effect in *TREK-1*$^{-/-}$ mice (**Table 1 N° 2F, G, H, I)**. We additionally assessed the effects of riluzole in mice treated with oxaliplatin + 5FU regime in order to provide an even closer clinically relevant preclinical evaluation for the effect of riluzole on oxaliplatin-induced neuropathic effect. Administration of oxaliplatin and 5-FU significantly decreased cold sensitivity thresholds in mice as soon as day 7 after the first administration up to the end of the experiment and riluzole significantly decreased the oxaliplatin + 5FU-induced cold hypersensitivity (**Suppl. data 3A, Table 1 N° Suppl. data 3A)**. Moreover, spadin significantly decreased riluzole-induced analgesic effect in oxaliplatin + 5FU-treated animals (**Suppl. data 3B, Table 1 N° Suppl. data 3B)**. Of note, riluzole (7.5 mg/kg, i.p.), used as a curative treatment, was also able to exert an analgesic effect at day 28 after repeated oxaliplatin administrations (**Suppl. data 4, Table 1 N° Suppl. data 4**).

3.3. Oxaliplatin induces delayed proprioceptive impairment that is prevented by riluzole

Proprioceptive impairment appears as a consequence of chronic cumulative oxaliplatin treatment (Cersosimo, 2005) and is an element of the dose-limiting toxicity of the drug (Grothey, 2005). Performance on the balance beam is a useful measure of fine coordination and balance (Brooks and Dunnett, 2009) that, to our knowledge, has never been used in preclinical models of oxaliplatin-induced neuropathy. During this test the animal stays upright and walks across an elevated narrow beam to a safe platform. Performance on the beam is quantified by measuring the time needed by the mouse to cross the beam and the number of paw slips that occur in the process. This task has been shown to be particularly useful for detecting subtle deficits in motor skills and balance that may not be detected by other motor tests, such as the rotarod. None of the two parameters, time to cross beam (fine coordination) (**Table 1 N° Suppl. data 5A**) and number

of paw slips (balance) (**Table 1 N° Suppl. data 5B**), were altered by oxaliplatin 7 days after the beginning of the treatment (**Suppl. data 5A-B**). At day 28 (end point) fine coordination **(Fig. 3 B, Table 1 N° 3B, and Fig. 3C, Table 1 N° 3C**) and balance **(Fig. 3 D, Table 1 N° 3D, and Fig. 3E, Table 1 N° 3E**) were altered in all oxaliplatin-treated mice**E).** Riluzole treatment (60 µg/mL, p.o) prevented balance deficits in *TREK-1*$^{+/+}$ mice **(Fig. 3D)** but not in *TREK-1*$^{-/-}$ mice **(Fig. 3E)**. We also used the adhesive removal test to measure dexterity (time-to-remove). While no alteration was observed at day 7 (**Suppl. data 5C, Table 1 N° Suppl. data 5C**), removal times were significantly increased in oxaliplatin-treated *TREK-1*$^{+/+}$ mice at day 28 **(Fig. 3F, Table 1 N° 3F)**, highlighting an alteration in dexterity due to repeated administration of the chemotherapeutic drug. Riluzole treatment prevented oxaliplatin-induced dexterity impairment in control mice. Oxaliplatin also induced deficits in dexterity in *TREK1*$^{-/-}$ mice without any beneficial effect of riluzole **(Fig. 3G, Table 1 N° 3G).**

3.4. Oxaliplatin-chemotherapy induces depression-like symptoms that are prevented by riluzole

Depression-like phenotype was assessed at day 28 (**Fig. 4A**) using two classical behavioral tests: the Forced-Swimming Test (FST) and the Novelty-Suppressed Feeding (NSF) test. First, in line with previous data obtained by the laboratory (Heurteaux et al., 2006b), a significant reduction of immobility time was observed in untreated TREK-1$^{-/-}$ mice in comparison to wild type animals suggesting that TREK-1 is indeed involved in this behavior. Whatever the test used and whatever the genotype, a depression-like phenotype was observed at day 28 in oxaliplatin-treated mice as evidenced by an increased immobilization time during FST and a significant increased time to feed during NSF. Riluzole treatment (60 µg/mL, p.o) significantly prevented the depression-like phenotype observed (**Fig. 4B, Table1 N° 4B and Fig. 4C, Table1 N° 4C**) in *TREK-1*$^{+/+}$ mice, but not in *TREK-1*$^{-/-}$ animals (**Fig. 4D, Table1 N° 4D and Fig. 4E, Table1 N° 4E**).

3.5. Oxaliplatin induces peripheral nerve functional and morphological alterations that are prevented by riluzole

Consistent with what has been previously shown (Renn et al., 2011; Wozniak et al., 2012), nerve conduction velocity (NCV) was found to be significantly decreased in the oxaliplatin-treated group as soon as day 7 (**Fig. 5A, Table1 N° 5A**) and this alteration is drastically augmented at day 28 (**Figure 5B, Table1 N° 5B**). DRG neurons with abnormal, excentred (**Table1 N° 5D**) and multi nucleoli (**Table1 N° 5E)** were also observed at day 28 (**Figure 5C-E**). Riluzole administration significantly prevented decrease of NCV both at day 7 and at day 28 (**Figure 5A-B**) and DRG morphological alterations observed at day 28 (**Figure 5C-E**). In accordance with those results, abnormal (degraded as well as vacuolated) mitochondria were also more frequently observed on sciatic nerves when the mice are treated with oxaliplatin and riluzole seems to prevent these ultrastructural abnormalities (**Suppl. data 6**).

3.6. Effect of riluzole on human colon cancer cell line viability

The effects of oxaliplatin and riluzole on two human colon cancer cell lines viabilities were determined after 48-h exposure of the drugs in both T84 and HT29 cells. MTT cell proliferation assays were done with different doses of oxaliplatin (1-32 μM) and riluzole (1-100 μM) for 48h. As expected, oxaliplatin induced a dose-dependent decrease in cell viability in both cell lines **(Fig. 6A-B).** Interestingly, riluzole also significantly reduced the viability of T84 cells from the lowest dose tested (1μM) (**Fig. 6A**) and the viability of HT29 cells for doses equal or higher than 50 μM (**Fig. 6B**). The important experiment was of course to assess the combined effect of oxaliplatin and riluzole on cell viability. Whatever the cell line, T84 (**Fig. 6E, Table1 N° 6E**) or HT29 (**Fig. 6F, Table1 N° 6F**), riluzole did not decrease the antiproliferative effect of oxaliplatin (**Fig. 6C-F**). We evaluated the effects of riluzole and oxaliplatin on apoptosis in both cell lines (Figure 6 G-H). After 48h of treatment, an apoptotic effect of oxaliplatin was observed both in T84 (**Table 1 N° 6G**) and HT29 (**Table 1 N° 6H**) cell lines. Riluzole alone did not exert significant effect on apoptosis neither in T84 nor in HT29 cells and did not affect oxaliplatin pro-apoptotic effect.

3.7. Riluzole does not alter the anticancer effect of oxaliplatin in $Apc^{Min/+}$ mice

To evaluate the effect of riluzole on the anticancer effect of oxaliplatin *in vivo*, we used the $Apc^{Min/+}$ model of intestinal neoplasia on the C57BL/6J background. This murine model harbors a germline mutation in the *Apc* gene at codon 850 that leads to a truncation of the protein (Moser et al., 1990). In $Apc^{Min/+}$ mice, adenomas begin to develop in infancy with death occurring at 16–20 weeks due to chronic intestinal hemorrhage (Shoemaker et al., 1995). First of all, we evaluated the effect of oxaliplatin and riluzole in cold sensitivity in this strain of mice. We observed a similar development of sensory neuropathic pain symptoms in $Apc^{Min/+}$ mice (**Fig. 7B, Table1 N° 7B**) and **(Fig. 7C, Table1 N° 7C**) as the ones observed in C57Bl/6J under the same treatment **(Fig. 2B, 2C)**. Riluzole administration (60 µg/mL, p.o) led to a partial reversion of peripheral cold symptoms and total reversion of orofacial cold hypersensitivity in $Apc^{Min/+}$. Spadin significantly decreased the riluzole-induced analgesic effect in $Apc^{Min/+}$ mice (**Suppl. data 7, Table1 N° Suppl. data 7**), suggesting again a pivotal role of the TREK-1 channel in the analgesic effect of riluzole. At day 28 after OIPN induction, mice were killed and the number of tumors in the colon (**Table1 N° 7D colon**), the duodenum and the jejunum (**Table1 N° 7D duod. + jejunum**) was quantified. Oxaliplatin treatment led to a strong decrease (73.7±9.7%) in the number of tumors in the entire intestinal tract **(Fig. 7D, Table1 N° Suppl. data 7D)**. Riluzole alone or together with oxaliplatin led to a significant anticancer effect as shown by the lower number of tumors observed in the small intestine. Analyses of colonic tumor sizes also show that riluzole did not reduce the effect of oxaliplatin (**Fig. 7E, Table1 N° Suppl. data 7E**).

4. Discussion

Oxaliplatin, a third generation platinum-based chemotherapy, is a central drug in the treatment of colorectal cancer (Andre et al., 2004). However, dose limiting neurotoxicity resulting from this chemotherapeutic treatment is a prominent feature with both acute and chronic manifestations

(Beijers et al., 2015; Pachman et al., 2015). Severe chronic sensory neuropathy develops in a large proportion of patients (Beijers et al., 2015).

We (Descoeur et al., 2011), and others (Grolleau et al., 2001), have previously demonstrated that acute neuropathic pain symptoms induced by oxaliplatin-chemotherapy could be due to changes in ion channel gene expression in DRG neurons. A particularly important effect of oxaliplatin is a drastic decrease of the expression (Descoeur et al., 2011) of the hyperpolarizing mechano-, osmo-, heat- and cold-sensitive TREK and TRAAK channels (Chemin et al., 2005; Maingret et al., 1999a; Maingret et al., 2000; Maingret et al., 1999b), that are involved in polymodal pain perception (Alloui et al., 2006; Noel et al., 2009; Pereira et al., 2014) four days after a single dose of oxaliplatin in mice, at the peak of pain hypersensitivity (Descoeur et al., 2011). On the other hand : (i) double knock-out animals for these channels exhibit an exaggerated cold sensitivity similar to oxaliplatin-treated animals (Noel et al., 2009) and (ii) oxaliplatin fails to induce cold hypersensitivity in these mice (Descoeur et al., 2011). We have shown previously that monomodal cold-specific fibers affected by oxaliplatin use TRPM8 as the mean detector of innocuous and noxious cold stimuli, and that oxaliplatin modifies their excitability by decreasing the expression level, i.e. inhibitor potential, of K2P channels (Descoeur et al., 2011) which, in combination with TRPM8 defined the cold threshold (Noel et al., 2009). We have also shown that polymodal cold and mechano-sensitive fibers affected by oxaliplatin also use TRPM8 as cold detector in addition to yet to be identified mechanosensors. Again, oxaliplatin induces in these fibers a downregulation of the cold and mechano-threshold controlling TREK-1 and TRAAK K2P channels. Mechano-sensitive fibers with up-regulated TRPA1 and downregulated TREK-1 and TRAAK channels in their mechanosensori-machinery convey oxaliplatin-mediated hypersensitivity (Descoeur et al., 2011). All these results taken together suggested a key role of TREK and/or TRAAK channels in oxaliplatin-induced pain symptoms.

The TREK/TRAAK potassium channels family serves the role of thermo-sensitive and mechano-sensitive brakes compensating the excitatory contribution of mechano- and thermo-sensitive excitatory channels (Noel et al., 2009). Oxaliplatin reduces in a drastic way the electrical silencing

potential of the TREK/TRAAK channels. Therefore, it immediately comes to mind that an activator of these TREK/TRAAK channels could compensate for their reduced expression and reinstore a more normal sensory perception.

There is one activator that seems ideal for this task. It is riluzole (Duprat et al., 2000; Lesage et al., 2000). It is an ideal drug because it has been approved in many countries, and used for a long time, for treatment of patients with amyotrophic lateral sclerosis. It is thought to prolong survival and is reasonably safe even at high doses of 100mg daily (Lacomblez et al., 1996). We have found that riluzole displays a marked analgesic effect against cold hypersensitivity induced by a single injection of oxaliplatin, and observed that this effect implies the specific activation of TREK-1 since it is lost only in TREK-1 knock-out animals. Elimination of the TREK-2 or TRAAK channels did not eliminate the curative effect of riluzole.

Chronic neurotoxicity that occurs with cumulative dosing of oxaliplatin, is often irreversible, and is associated with high morbidity and decreased quality of life many years after treatment completion. That is why we developed a model of neuropathy induced by repeated oxaliplatin injections that mimicked, in a translational perspective, sustained neuropathic pain symptoms, as well as delayed sensory-motor alterations and depression-like symptoms observed in patients treated by this anticancer agent. Riluzole partly or totally prevented both cephalic and extracephalic pain symptoms in oxaliplatin-treated animals. The analgesic efficacy of riluzole, again, involves TREK-1 channel action at both locations. In addition, riluzole also prevented proprioceptive alterations (balance and dexterity) observed in mice after repeated oxaliplatin injections. A neuroprotective effect of riluzole could account for its beneficial effect in oxaliplatin-treated animals, as suggested by the ultrastructural and electrophysiological results we obtained. Concomitantly with mechanical hyperalgesia, decreased intraepidermal nerve fibers has been observed in oxaliplatin-treated animals (Boyette-Davis and Dougherty, 2011). The neuroprotective effect of riluzole might also involve intraepidermal nerve fibers preservation. The most likely interpretation is that the drastic early occurring beneficial effect of riluzole on oxaliplatin induced sensory dysfunction and pain, results in a strong attenuation of depression

like symptoms, as well as proprioceptive defects in chronic treatments. All our results also demonstrate that TREK-1 is a central contributor of all beneficial effects of riluzole in this model of chronic neuropathic pain.

This paper also demonstrates that there is a late phase development of a depression-like phenotype in mice treated with oxaliplatin. This observation reinforces the clinical relevance of our model since depressive symptoms are also observed in oxaliplatin-treated patients (Tofthagen et al., 2013). These depressive-like disorders were suppressed by riluzole, thus reinforcing the potential interest of this drug in this pathological context. Once more the effect of riluzole was lost in TREK-1$^{-/-}$ mice. Clearly, the TREK-1 channel is not involved in the development of the depressive state induced by oxaliplatin because the chemotherapeutic drug in chronic treatment induces depression in both TREK-1$^{+/+}$ and TREK-1$^{-/-}$ mice. Interestingly, although riluzole is not currently used in psychiatry. it has been considered for the treatment of mood and anxiety disorders in humans (Pittenger et al., 2008).

Antidepressant effect of riluzole has also been observed in other mice models (Gourley et al., 2012a). One particularly interesting model is associated with chronic exposure to corticosterone. This treatment produces severe motivational deficits that are corrected by riluzole (Gourley et al., 2012b). It is particularly interesting to observe that two very stressful treatment, i.e. corticosterone (Gourley et al., 2012b) and oxaliplatin (this work) induce depressive states that are both corrected by riluzole. The beneficial effect of riluzole observed by Gourley et al (Gourley et al., 2012b) has been attributed to restoration of prefrontal BDNF expression after corticosterone. This is an important observation. The brain neurotrophin system might also be compromised in chronically treated oxaliplatin mice or humans, with the associated pain situation, and, if this happens, riluzole could also restore normal BDNF levels. In such a case, considering the present results, it would probably imply that the BDNF effect would be subsequent to riluzole activation of the TREK-1 channel.

Overall, reinforced by the very low toxicity and good tolerability of riluzole in humans (Lacomblez et al., 1996), these results strongly encourage a use of riluzole in association with oxaliplatin for

the prevention of oxaliplatin-induced neuronal adverse side effects and comorbidities. The known side effects of riluzole alone (mainly gastrointestinal disturbances and asthenia) seem to be limited both in intensity and in frequency and hopefully will not be accentuated in oxaliplatin treatment of humans. One important question remained to be answered: does riluzole have any effect on the anticancer oxaliplatin treatment? In fact we observed a decreased survival rate, i.e. a beneficial anticancer effect, on both human colorectal cancer cell lines T84 and HT29 after riluzole treatment. Interestingly, this effect of riluzole treatment has been observed for several other cancer cell types (Yamamoto et al., 2017) including melanoma, glioma and prostate (Akamatsu et al., 2009; Le et al., 2010; Yohay et al., 2014). More important, riluzole had no negative effects on the chemotherapeutic action of oxaliplatin. It could even act as a potentiator. Along these lines, results obtained with $APC^{Min/+}$ which harbor a defined genetic etiology that closely mimics the mechanism of *APC* gene inactivation observed in Familial Adenomatous Polyposis and most sporadic human colon adenomas, are particularly instructive. In these mice, riluzole also corrected the deleterious sensory perception effects of oxaliplatin and not only riluzole did not hamper the antitumoral effect of oxaliplatin in colon duodenum and jejunum, but even improved it. Hence, riluzole alone or together with oxaliplatin led to a significant anticancer effect as shown by the lower number of tumors observed in the small intestine, while it did not reduce per se the size of, presumably more undifferentiated, tumors. This is in accordance with the stronger effect of riluzole on HT29 (a primary colon derived-) than in T84 (a colon lung metastasis derived-) cells lines viability. Thus, riluzole could have antineoplasic effect on early stages rather than on late stages of colon cancer development.

In conclusion, because riluzole has long been used for amyotrophic lateral sclerosis patients, and during long periods of time for each patient with a good tolerability, because it does not negatively alter, but rather improves, the anti-cancer activity of oxaliplatin, it should be tested in a combined therapy with oxaliplatin to prevent or decrease the negative effects associated with the neuropathy inducing action of oxaliplatin. Moreover the systematic involvement of TREK1 in these positive effects highlights the interest of this channel as a pharmacological target for anti-

neuropathic drug. This result is in line with the growing interest of ion channels as new target for both neuropathic pain and cancer therapies (Luiz and Wood, 2016; Pardo and Stuhmer, 2014; Raouf et al., 2010; Tsantoulas et al., 2017; Viana et al., 2002).

Acknowledgments

The authors have no conflict of interest to declare.

The authors wish to thank Mathilde Bonnet for providing T84 and HT29 cells as well as *Apc*$^{Min/+}$ mice, Marc Borsotto for kindly providing spadin, for reading the manuscript and for helpful discussions, and James J. Cox for pertinent advice and proofreading of the article. We thank Szczepaniak, Blavignac and Novais-Gameiro (Center for Medical Cell Imaging (CICS) of University Clermont Auvergne) for their technical assistance concerning the histological and morphological study. We thank Jérémy Pinguet (CHU Clermont-Ferrand) for riluzole titration assay. This work was supported by Inserm, Clermont Auvergne University, CAP 20-25 project, grants from Agence Nationale de la Recherche (ANR-13-BSV1-0006-03), Fondation pour la Recherche sur le Cerveau, the Société Française d'Etude et de Traitement de la Douleur, région Auvergne and FEDER.

Author contributions

L.Poupon, S.Lamoine, M.M., S.Lolignier and V.P. conducted experiments, analyzed the data and participated to the preparation of the manuscript. D.A.B., Y.A., M.M., F.G. and L.Prival participated to experiments. S.Lolignier, N.K., N.A. and D.B. were associated with the design and analysis of the research. J.B., A.E. and M.L. designed research, supervised the project, participated in data analysis and wrote the paper.

Figure 1: Riluzole causes an analgesic effect that involves the TREK-1 channel action in an acute model of OIPN. After baseline latency recordings, kinetics of the antihyperalgesic effect of riluzole (7.5 mg/kg, i.p.) were assessed 4 days after oxaliplatin injection (6 mg/kg, ip) in mice

deleted or not for TREK-1 (A), TREK-2 (B) or TRAAK (C) channels using the tail immersion test (10°C). Pre- and post- (15, 30, 45, 60 and 90 min after) treatment withdrawal latencies were assessed. Data are represented, on the left panels, as the mean±s.e.m of withdrawal latencies and, on the right panels, as the mean±s.e.m. of the areas under the time course curves (AUC, s.min) to investigate global effects. Area under the time-course (0–90 minutes) curve (AUC) of withdrawal latencies variations post-riluzole administration were calculated by the trapezoidal rule and expressed as means ± SEM of values obtained from 8 to 10 mice per group. The pharmacological blockade of the TREK-1 channel using spadin also prevents the anti-hyperalgesic effect of riluzole (D). At day 4, C57Bl/6JRj mice were injected either with riluzole (7.5 mg/kg, i.p.) or saline (NaCl 0.9%) 30 minutes after systemic spadin injection (1 mg/kg, sc.). Pre- and post- (15, 30, 45, 60 and 90 min after) treatment withdrawal latencies were measured. Data are represented as the time-course of withdrawal latencies and as the mean ± SEM. of AUC (n=9-10 per group). Statistical analysis was performed using a two-way repeated measure analysis of variance (RM ANOVA) for data of the kinetics of withdrawal latencies and a two-way analysis of variance (ANOVA) for data of the AUCs, , detailed in Table 1, and a Bonferroni post hoc test; *, $p < 0.05$, **, $p < 0.01$, ***, $p < 0.001$, wild-type littermate mice vehicle *versus* wild-type littermate mice riluzole; ¤, $p < 0.05$, ¤¤, $p < 0.001$, ¤¤¤, $p < 0.0001$, KO mice vehicle *versus* KO mice- riluzole ; $$$, $p < 0.001$, KO mice riluzole *versus* wild-type littermate mice- riluzole.

<u>Figure 2:</u> Riluzole prevents oxaliplatin-induced chronic neuropathic pain. (A) Experimental design: *TREK-1*$^{-/-}$ mice or their wild-type littermates received oxaliplatin (6 mg/kg, i.p.) or vehicle (Glucose 5%) twice a week for 4 weeks. Riluzole (60 µg/mL) was administered in the drinking water from day 0 to 28. Whatever the genotype, thermal cold pain hypersensitivity developed as soon as after day 7 in oxaliplatin treated group both at the extracephalic (B, F) and cephalic (C, G) levels. Similarly, mechanical pain hypersensitivity also developed in oxaliplatin-treated mice both at the extracephalic (D, H) and cephalic (E, I) levels. Riluzole significantly prevented oxaliplatin-induced pain hypersensitivity in *TREK-1*$^{+/+}$ mice but not in *TREK-1*$^{-/-}$ animals. Values are mean ±

SEM (n=4-10 per group). Statistical analysis was performed using a two-way repeated measure analysis of variance (RM ANOVA), detailed in Table 1, and a Bonferroni post hoc test; *, $p < 0.05$, **, $p < 0.01$, ***, $p < 0.001$, vehicle *versus* oxaliplatin; ¤, $p < 0.05$, ¤¤, $p < 0.01$, ¤¤¤, $p < 0.001$, oxaliplatin *versus* oxaliplatin + riluzole; $, $p < 0.05$, $$, $p < 0.01$, $$$, $p < 0.001$, vehicle *versus* oxaliplatin + riluzole; #, $p < 0.05$, ##, $p < 0.01$, ###, $p < 0.001$, changes from baseline for the oxaliplatin group; Ɛ, $p < 0.05$, ƐƐ , $p < 0.01$, ƐƐƐ, $p < 0.001$, changes from baseline for the oxaliplatin + riluzole group.

Figure 3: Repeated oxaliplatin treatment leads to sensori-motor deficits that are prevented by riluzole. (A) Experimental design. Fine motor coordination (B, C), balance (D, E), and dexterity (F, G) were assessed using the beam walking and the adhesive removal tests at day 28 after repeated injections of oxaliplatin (6 mg/kg, twice a week for four weeks) with or without riluzole treatment (60 µg/mL in the drinking water) in *TREK-1*$^{+/+}$ and *TREK-1*$^{-/-}$ mice. Values are mean ± SEM (n=5-10 per group). NS: not significant. Statistical analysis was performed using a two-way analysis of variance (ANOVA), detailed in Table 1, and a Bonferroni post hoc test; *, $p < 0.05$, **, $p < 0.01$, ***, $p < 0.001$, *versus* the vehicle group; ¤, $p < 0.05$, ¤¤, $p < 0.01$, oxaliplatin *versus* oxaliplatin + riluzole.

Figure 4: Riluzole prevents the depression-like phenotype in the late phase of chronic OIPN. (A) Experimental design. *TREK-1*$^{+/+}$ and *TREK-1*$^{-/-}$ mice were subjected to a Forced Swimming Test (FST) (B, D) and the Novelty-Suppressed Feeding (NSF) (C, E) test at endpoint (day 28) after vehicle or oxaliplatin (6 mg/kg) twice a week with or without riluzole in the drinking water (60 µg/mL) for 4 weeks. Values are mean ± SEM (n=5-10 per group). Statistical analysis was performed using a two-way analysis of variance (ANOVA), detailed in Table 1, and a Bonferroni post hoc test; *, $p < 0.05$, **, $p < 0.01$, ***, $p < 0.001$, *versus* the vehicle group; ¤, $p < 0.05$, ¤¤, $p < 0.01$, oxaliplatin *versus* oxaliplatin + riluzole.

Figure 5: Riluzole prevents oxaliplatin-induced peripheral nerve functional and morphological alterations. Oxaliplatin significantly decreased caudal nerve conduction in mice both at day 7 (A) and at day 28 (B). Riluzole significantly prevents this oxaliplatin-induced functional deficit (A-B). Values are expressed as mean ± SEM (n = 9-14). Images of L4-L6 DRG neurons sections from C57Bl/6JRj mice treated or not with oxaliplatin and or riluzole at day 28 (scale bars = 50µm). Arrowhead indicates neurons with excentred nuclei and multiple nucleoli (C). Quantification of DRG multiple nucleoli (D) and excentric nucleoli (E). Values are expressed as mean ± SEM (n = 9-11). Statistical analysis was performed using two-way ANOVA, detailed in Table 1, with Bonferoni post-hoc test; * for p<0,05; ** for 0.01; *** p<0,001, versus the vehicle group.

Figure 6: Riluzole does not affect oxaliplatin-induced cytotoxic effect in human colon cancer cell lines. Oxaliplatin and riluzole dose-dependently inhibited survival of T84 (A) and HT29 (B) colorectal cancer cells as measured by inhibition of mitochondrial dehydrogenase activity (MTT assay). At the dose of 50 µM, riluzole did not alter the cytostatic effect of oxaliplatin (16 µM) in both cell lines as observed by MTT assay (C-F). At the same doses, oxaliplatin exert an apoptotic effect both in T84 (G) and HT29 (H) cell lines. Riluzole alone did not exert significant effect on apoptosis neither in T84 nor in HT29 cells and did not impact oxaliplatin pro-apoptotic effect. The average results from at least three independent experiments are presented. Values are expressed as mean ± SEM. Statistical analysis was performed using two-way ANOVA, detailed in Table 1, with Bonferonni post-hoc test; * for p<0,05; ** for 0.01; *** p<0,001, versus the vehicle group; ° for p<0.05, °°° for p<0.001, versus the oxaliplatin group; ¤ for p<0.05, ¤¤ for p<0.01, ¤¤¤ for p<0.001, versus the riluzole group.

Figure 7: Oxaliplatin-induced anti tumoral effect in *Apc*$^{Min/+}$ mice is not altered by riluzole. (A) Experimental design. Cephalic and extracephalic cold pain sensitivity was evaluated in 4 groups of *Apc*$^{Min/+}$ mice: vehicle-treated group, riluzole-treated group, oxaliplatin-treated group

and oxaliplatin- + riluzole-treated group (B, C). Mice received oxaliplatin (6 mg/kg, i.p.) or vehicle (Glucose 5%) twice a week for 4 weeks. Riluzole (60 µg/mL) was administered in the drinking water. Values are mean ± SEM (n=8 per group). Statistical analysis was performed using a two-way repeated measure analysis of variance (RM ANOVA), detailed in Table 1, and a Bonferroni post hoc test; *, $p < 0.05$, **, $p < 0.01$, ***, $p < 0.001$, vehicle *versus* oxaliplatin; ¤, $p < 0.05$, ¤¤, $p < 0.01$, ¤¤¤, $p < 0.001$, oxaliplatin *versus* oxaliplatin + riluzole. At end point (day 28), mouse intestinal tract was removed and the number of intestinal tumors counted in the duodenum, the jejunum and the colon (D). Colonic tumor volume was also measured (E). Values are mean ± SEM (n=8 per group). Statistical analysis was performed using a two-way analysis of variance (ANOVA), detailed in Table 1, and a Bonferroni post hoc test; *, $p < 0.05$, **, $p < 0.01$, ***, $p < 0.001$, *versus* the vehicle group.

References

Akamatsu, K., Shibata, M. A., Ito, Y., Sohma, Y., Azuma, H., Otsuki, Y., 2009. Riluzole induces apoptotic cell death in human prostate cancer cells via endoplasmic reticulum stress. Anticancer Res 29, 2195-2204.

Alloui, A., Zimmermann, K., Mamet, J., Duprat, F., Noel, J., Chemin, J., Guy, N., Blondeau, N., Voilley, N., Rubat-Coudert, C., Borsotto, M., Romey, G., Heurteaux, C., Reeh, P., Eschalier, A., Lazdunski, M., 2006. TREK-1, a K+ channel involved in polymodal pain perception. Embo J 25, 2368-2376.

Andre, T., Boni, C., Mounedji-Boudiaf, L., Navarro, M., Tabernero, J., Hickish, T., Topham, C., Zaninelli, M., Clingan, P., Bridgewater, J., Tabah-Fisch, I., de Gramont, A., 2004. Oxaliplatin, fluorouracil, and leucovorin as adjuvant treatment for colon cancer. N Engl J Med 350, 2343-2351.

Bayliss, D. A., Barrett, P. Q., 2008. Emerging roles for two-pore-domain potassium channels and their potential therapeutic impact. Trends Pharmacol Sci 29, 566-575.

Beijers, A. J., Mols, F., Tjan-Heijnen, V. C., Faber, C. G., van de Poll-Franse, L. V., Vreugdenhil, G., 2015. Peripheral neuropathy in colorectal cancer survivors: the influence of oxaliplatin administration. Results from the population-based PROFILES registry. Acta Oncol 54, 463-469.

Benveniste, H., Drejer, J., Schousboe, A., Diemer, N. H., 1984. Elevation of the extracellular concentrations of glutamate and aspartate in rat hippocampus during transient cerebral ischemia monitored by intracerebral microdialysis. J Neurochem 43, 1369-1374.

Binder, A., Stengel, M., Maag, R., Wasner, G., Schoch, R., Moosig, F., Schommer, B., Baron, R., 2007. Pain in oxaliplatin-induced neuropathy--sensitisation in the peripheral and central nociceptive system. Eur J Cancer 43, 2658-2663.

Bouet, V., Boulouard, M., Toutain, J., Divoux, D., Bernaudin, M., Schumann-Bard, P., Freret, T., 2009. The adhesive removal test: a sensitive method to assess sensorimotor deficits in mice. Nat Protoc 4, 1560-1564.

Boyette-Davis, J., Dougherty, P. M., 2011. Protection against oxaliplatin-induced mechanical hyperalgesia and intraepidermal nerve fiber loss by minocycline. Exp Neurol 229, 353-357.

Brohawn, S. G., Campbell, E. B., MacKinnon, R., 2014. Physical mechanism for gating and mechanosensitivity of the human TRAAK K+ channel. Nature 516, 126-130.

Brooks, S. P., Dunnett, S. B., 2009. Tests to assess motor phenotype in mice: a user's guide. Nat Rev Neurosci 10, 519-529.

Busserolles, J., Alloui, A., Lazdunski, M., Eschalier, A., 2010. Use of riluzole for treating or preventing the adverse effects of antineoplastic agents. US9511045B2.
Cavaletti, G., Tredici, G., Petruccioli, M. G., Donde, E., Tredici, P., Marmiroli, P., Minoia, C., Ronchi, A., Bayssas, M., Etienne, G. G., 2001. Effects of different schedules of oxaliplatin treatment on the peripheral nervous system of the rat. Eur J Cancer 37, 2457-2463.
Cersosimo, R. J., 2005. Oxaliplatin-associated neuropathy: a review. Ann Pharmacother 39, 128-135.
Chemin, J., Patel, A. J., Duprat, F., Lauritzen, I., Lazdunski, M., Honore, E., 2005. A phospholipid sensor controls mechanogating of the K+ channel TREK-1. Embo J 24, 44-53.
Choi, D. W., Rothman, S. M., 1990. The role of glutamate neurotoxicity in hypoxic-ischemic neuronal death. Annu Rev Neurosci 13, 171-182.
Choi, Y., Yoon, Y. W., Na, H. S., Kim, S. H., Chung, J. M., 1994. Behavioral signs of ongoing pain and cold allodynia in a rat model of neuropathic pain. Pain 59, 369-376.
Descoeur, J., Pereira, V., Pizzoccaro, A., Francois, A., Ling, B., Maffre, V., Couette, B., Busserolles, J., Courteix, C., Noel, J., Lazdunski, M., Eschalier, A., Authier, N., Bourinet, E., 2011. Oxaliplatin-induced cold hypersensitivity is due to remodelling of ion channel expression in nociceptors. EMBO Mol Med 3, 266-278.
Di Cesare Mannelli, L., Pacini, A., Bonaccini, L., Zanardelli, M., Mello, T., Ghelardini, C., 2013. Morphologic features and glial activation in rat oxaliplatin-dependent neuropathic pain. J Pain 14, 1585-1600.
Dong, Y. Y., Pike, A. C., Mackenzie, A., McClenaghan, C., Aryal, P., Dong, L., Quigley, A., Grieben, M., Goubin, S., Mukhopadhyay, S., Ruda, G. F., Clausen, M. V., Cao, L., Brennan, P. E., Burgess-Brown, N. A., Sansom, M. S., Tucker, S. J., Carpenter, E. P., 2015. K2P channel gating mechanisms revealed by structures of TREK-2 and a complex with Prozac. Science 347, 1256-1259.
Duprat, F., Lesage, F., Patel, A. J., Fink, M., Romey, G., Lazdunski, M., 2000. The neuroprotective agent riluzole activates the two P domain K(+) channels TREK-1 and TRAAK. Mol Pharmacol 57, 906-912.
Enyedi, P., Czirjak, G., 2010. Molecular background of leak K+ currents: two-pore domain potassium channels. Physiol Rev 90, 559-605.
Ettaiche, M., Fillacier, K., Widmann, C., Heurteaux, C., Lazdunski, M., 1999. Riluzole improves functional recovery after ischemia in the rat retina. Invest Ophthalmol Vis Sci 40, 729-736.
Gourley, S. L., Espitia, J. W., Sanacora, G., Taylor, J. R., 2012a. Antidepressant-like properties of oral riluzole and utility of incentive disengagement models of depression in mice. Psychopharmacology (Berl) 219, 805-814.
Gourley, S. L., Swanson, A. M., Jacobs, A. M., Howell, J. L., Mo, M., Dileone, R. J., Koleske, A. J., Taylor, J. R., 2012b. Action control is mediated by prefrontal BDNF and glucocorticoid receptor binding. Proc Natl Acad Sci U S A 109, 20714-20719.
Groeneveld, G. J., van Kan, H. J., Lie, A. H. L., Guchelaar, H. J., van den Berg, L. H., 2008. An association study of riluzole serum concentration and survival and disease progression in patients with ALS. Clin Pharmacol Ther 83, 718-722.
Grolleau, F., Gamelin, L., Boisdron-Celle, M., Lapied, B., Pelhate, M., Gamelin, E., 2001. A possible explanation for a neurotoxic effect of the anticancer agent oxaliplatin on neuronal voltage-gated sodium channels. J Neurophysiol 85, 2293-2297.
Grothey, A., 2005. Clinical management of oxaliplatin-associated neurotoxicity. Clin Colorectal Cancer 5 Suppl 1, S38-46.
Gurney, M. E., Cutting, F. B., Zhai, P., Doble, A., Taylor, C. P., Andrus, P. K., Hall, E. D., 1996. Benefit of vitamin E, riluzole, and gabapentin in a transgenic model of familial amyotrophic lateral sclerosis. Ann Neurol 39, 147-157.
Hartmann, J. T., Lipp, H. P., 2003. Toxicity of platinum compounds. Expert Opin Pharmacother 4, 889-901.
Hershman, D. L., Lacchetti, C., Dworkin, R. H., Lavoie Smith, E. M., Bleeker, J., Cavaletti, G., Chauhan, C., Gavin, P., Lavino, A., Lustberg, M. B., Paice, J., Schneider, B., Smith, M. L., Smith, T., Terstriep, S., Wagner-Johnston, N., Bak, K., Loprinzi, C. L., 2014. Prevention and management of chemotherapy-

induced peripheral neuropathy in survivors of adult cancers: American Society of Clinical Oncology clinical practice guideline. J Clin Oncol 32, 1941-1967.
Heurteaux, C., Guy, N., Laigle, C., Blondeau, N., Duprat, F., Mazzuca, M., Lang-Lazdunski, L., Widmann, C., Zanzouri, M., Romey, G., Lazdunski, M., 2004. TREK-1, a K+ channel involved in neuroprotection and general anesthesia. Embo J 23, 2684-2695.
Heurteaux, C., Laigle, C., Blondeau, N., Jarretou, G., Lazdunski, M., 2006a. Alpha-linolenic acid and riluzole treatment confer cerebral protection and improve survival after focal brain ischemia. Neuroscience 137, 241-251.
Heurteaux, C., Lucas, G., Guy, N., El Yacoubi, M., Thummler, S., Peng, X. D., Noble, F., Blondeau, N., Widmann, C., Borsotto, M., Gobbi, G., Vaugeois, J. M., Debonnel, G., Lazdunski, M., 2006b. Deletion of the background potassium channel TREK-1 results in a depression-resistant phenotype. Nat Neurosci 9, 1134-1141.
Janssen, P. A., Niemegeers, C. J., Dony, J. G., 1963. The inhibitory effect of fentanyl and other morphine-like analgesics on the warm water induced tail withdrawl reflex in rats. Arzneimittelforschung 13, 502-507.
Lacomblez, L., Bensimon, G., Leigh, P. N., Guillet, P., Meininger, V., 1996. Dose-ranging study of riluzole in amyotrophic lateral sclerosis. Amyotrophic Lateral Sclerosis/Riluzole Study Group II. Lancet 347, 1425-1431.
Lang-Lazdunski, L., Heurteaux, C., Mignon, A., Mantz, J., Widmann, C., Desmonts, J., Lazdunski, M., 2000. Ischemic spinal cord injury induced by aortic cross-clamping: prevention by riluzole. Eur J Cardiothorac Surg 18, 174-181.
Lang-Lazdunski, L., Heurteaux, C., Vaillant, N., Widmann, C., Lazdunski, M., 1999. Riluzole prevents ischemic spinal cord injury caused by aortic crossclamping. J Thorac Cardiovasc Surg 117, 881-889.
Le, M. N., Chan, J. L., Rosenberg, S. A., Nabatian, A. S., Merrigan, K. T., Cohen-Solal, K. A., Goydos, J. S., 2010. The glutamate release inhibitor Riluzole decreases migration, invasion, and proliferation of melanoma cells. J Invest Dermatol 130, 2240-2249.
Lesage, F., 2003. Pharmacology of neuronal background potassium channels. Neuropharmacology 44, 1-7.
Lesage, F., Lazdunski, M., 2000. Molecular and functional properties of two-pore-domain potassium channels. Am J Physiol Renal Physiol 279, F793-801.
Lesage, F., Terrenoire, C., Romey, G., Lazdunski, M., 2000. Human TREK2, a 2P domain mechano-sensitive K+ channel with multiple regulations by polyunsaturated fatty acids, lysophospholipids, and Gs, Gi, and Gq protein-coupled receptors. J Biol Chem 275, 28398-28405.
Louzada-Junior, P., Dias, J. J., Santos, W. F., Lachat, J. J., Bradford, H. F., Coutinho-Netto, J., 1992. Glutamate release in experimental ischaemia of the retina: an approach using microdialysis. J Neurochem 59, 358-363.
Luiz, A. P., Wood, J. N., 2016. Sodium Channels in Pain and Cancer: New Therapeutic Opportunities. Adv Pharmacol 75, 153-178.
Maingret, F., Fosset, M., Lesage, F., Lazdunski, M., Honore, E., 1999a. TRAAK is a mammalian neuronal mechano-gated K+ channel. J Biol Chem 274, 1381-1387.
Maingret, F., Lauritzen, I., Patel, A. J., Heurteaux, C., Reyes, R., Lesage, F., Lazdunski, M., Honore, E., 2000. TREK-1 is a heat-activated background K(+) channel. Embo J 19, 2483-2491.
Maingret, F., Patel, A. J., Lesage, F., Lazdunski, M., Honore, E., 1999b. Mechano- or acid stimulation, two interactive modes of activation of the TREK-1 potassium channel. J Biol Chem 274, 26691-26696.
Mathie, A., Veale, E. L., 2007. Therapeutic potential of neuronal two-pore domain potassium-channel modulators. Curr Opin Investig Drugs 8, 555-562.
Mazella, J., Petrault, O., Lucas, G., Deval, E., Beraud-Dufour, S., Gandin, C., El-Yacoubi, M., Widmann, C., Guyon, A., Chevet, E., Taouji, S., Conductier, G., Corinus, A., Coppola, T., Gobbi, G., Nahon, J. L., Heurteaux, C., Borsotto, M., 2010. Spadin, a sortilin-derived peptide, targeting rodent TREK-1 channels: a new concept in the antidepressant drug design. PLoS Biol 8, e1000355.
Moser, A. R., Pitot, H. C., Dove, W. F., 1990. A dominant mutation that predisposes to multiple intestinal neoplasia in the mouse. Science 247, 322-324.

Nishizawa, Y., 2001. Glutamate release and neuronal damage in ischemia. Life Sci 69, 369-381.
Noel, J., Zimmermann, K., Busserolles, J., Deval, E., Alloui, A., Diochot, S., Guy, N., Borsotto, M., Reeh, P., Eschalier, A., Lazdunski, M., 2009. The mechano-activated K+ channels TRAAK and TREK-1 control both warm and cold perception. Embo J 28, 1308-1318.
Pachman, D. R., Qin, R., Seisler, D. K., Smith, E. M., Beutler, A. S., Ta, L. E., Lafky, J. M., Wagner-Johnston, N. D., Ruddy, K. J., Dakhil, S., Staff, N. P., Grothey, A., Loprinzi, C. L., 2015. Clinical Course of Oxaliplatin-Induced Neuropathy: Results From the Randomized Phase III Trial N08CB (Alliance). J Clin Oncol 33, 3416-3422.
Pardo, L. A., Stuhmer, W., 2014. The roles of K(+) channels in cancer. Nat Rev Cancer 14, 39-48.
Park, S. B., Goldstein, D., Lin, C. S., Krishnan, A. V., Friedlander, M. L., Kiernan, M. C., 2009a. Acute abnormalities of sensory nerve function associated with oxaliplatin-induced neurotoxicity. J Clin Oncol 27, 1243-1249.
Park, S. B., Lin, C. S., Krishnan, A. V., Goldstein, D., Friedlander, M. L., Kiernan, M. C., 2009b. Oxaliplatin-induced neurotoxicity: changes in axonal excitability precede development of neuropathy. Brain 132, 2712-2723.
Patel, A. J., Honore, E., Maingret, F., Lesage, F., Fink, M., Duprat, F., Lazdunski, M., 1998. A mammalian two pore domain mechano-gated S-like K+ channel. Embo J 17, 4283-4290.
Pereira, V., Busserolles, J., Christin, M., Devilliers, M., Poupon, L., Legha, W., Alloui, A., Aissouni, Y., Bourinet, E., Lesage, F., Eschalier, A., Lazdunski, M., Noel, J., 2014. Role of the TREK2 potassium channel in cold and warm thermosensation and in pain perception. Pain 155, 2534-2544.
Pittenger, C., Coric, V., Banasr, M., Bloch, M., Krystal, J. H., Sanacora, G., 2008. Riluzole in the treatment of mood and anxiety disorders. CNS Drugs 22, 761-786.
Porsolt, R. D., Bertin, A., Jalfre, M., 1977. Behavioral despair in mice: a primary screening test for antidepressants. Arch Int Pharmacodyn Ther 229, 327-336.
Raouf, R., Quick, K., Wood, J. N., 2010. Pain as a channelopathy. J Clin Invest 120, 3745-3752.
Reagan-Shaw, S., Nihal, M., Ahmad, N., 2008. Dose translation from animal to human studies revisited. Faseb J 22, 659-661.
Renn, C. L., Carozzi, V. A., Rhee, P., Gallop, D., Dorsey, S. G., Cavaletti, G., 2011. Multimodal assessment of painful peripheral neuropathy induced by chronic oxaliplatin-based chemotherapy in mice. Mol Pain 7, 29.
Santarelli, L., Saxe, M., Gross, C., Surget, A., Battaglia, F., Dulawa, S., Weisstaub, N., Lee, J., Duman, R., Arancio, O., Belzung, C., Hen, R., 2003. Requirement of hippocampal neurogenesis for the behavioral effects of antidepressants. Science 301, 805-809.
Shoemaker, A. R., Moser, A. R., Dove, W. F., 1995. N-ethyl-N-nitrosourea treatment of multiple intestinal neoplasia (Min) mice: age-related effects on the formation of intestinal adenomas, cystic crypts, and epidermoid cysts. Cancer Res 55, 4479-4485.
Simpson, R. K., Jr., Robertson, C. S., Goodman, J. C., 1990. Spinal cord ischemia-induced elevation of amino acids: extracellular measurement with microdialysis. Neurochem Res 15, 635-639.
Tofthagen, C., Donovan, K. A., Morgan, M. A., Shibata, D., Yeh, Y., 2013. Oxaliplatin-induced peripheral neuropathy's effects on health-related quality of life of colorectal cancer survivors. Support Care Cancer 21, 3307-3313.
Tsantoulas, C., Lainez, S., Wong, S., Mehta, I., Vilar, B., McNaughton, P. A., 2017. Hyperpolarization-activated cyclic nucleotide-gated 2 (HCN2) ion channels drive pain in mouse models of diabetic neuropathy. Sci Transl Med 9, eaam6072.
Viana, F., de la Pena, E., Belmonte, C., 2002. Specificity of cold thermotransduction is determined by differential ionic channel expression. Nat Neurosci 5, 254-260.
Wozniak, K. M., Wu, Y., Vornov, J. J., Lapidus, R., Rais, R., Rojas, C., Tsukamoto, T., Slusher, B. S., 2012. The orally active glutamate carboxypeptidase II inhibitor E2072 exhibits sustained nerve exposure and attenuates peripheral neuropathy. J Pharmacol Exp Ther 343, 746-754.
Wu, X., Liu, Y., Chen, X., Sun, Q., Tang, R., Wang, W., Yu, Z., Xie, M., 2013. Involvement of TREK-1 activity in astrocyte function and neuroprotection under simulated ischemia conditions. J Mol Neurosci 49, 499-506.

Wu, Y., Satkunendrarajah, K., Fehlings, M. G., 2014. Riluzole improves outcome following ischemia-reperfusion injury to the spinal cord by preventing delayed paraplegia. Neuroscience 265, 302-312.
Yamamoto, S., Ushio, S., Egashira, N., Kawashiri, T., Mitsuyasu, S., Higuchi, H., Ozawa, N., Masuguchi, K., Ono, Y., Masuda, S., 2017. Excessive spinal glutamate transmission is involved in oxaliplatin-induced mechanical allodynia: a possibility for riluzole as a prophylactic drug. Sci Rep 7, 9661.
Yohay, K., Tyler, B., Weaver, K. D., Pardo, A. C., Gincel, D., Blakeley, J., Brem, H., Rothstein, J. D., 2014. Efficacy of local polymer-based and systemic delivery of the anti-glutamatergic agents riluzole and memantine in rat glioma models. J Neurosurg 120, 854-863.

Table 1

FIGURE NUMBER	TEST USED?	n = ?	DEFINED?	REPORTED?	ANOVA MAIN EFFECTS	P VALUE	DEGREE OF FREEDOM & F/t/z/R etc value	SECTION & PARAGRAPH
1A kinetics	Two-way RM ANOVA	10 per group	mice from 4 groups	mean +/- SM	TREATMENT TIME INTERACTION	p < 0.0001 p < 0.0001 p < 0.0001	F(3.36) = 9.627 F(6.216) = 18.21 F(18.216) = 5.964	Fig. legend
1A AUC	Two-way ANOVA	10 per group	mice from 4 groups	mean +/- SM	GENOTYPE TREATMENT INTERACTION	p = 0.0001 p = 0.0115 p = 0.032	F(1.35) = 19 F(1.35) = 7.11 F(1.35) = 4.988	Fig. legend
1B Kinetics	Two-way RM ANOVA	8-9 per goup	mice from 4 groups	mean +/- SM	TREATMENT TIME INTERACTION	p < 0.0001 p < 0.0001 p < 0.0001	F(3.3) = 17.99 F(6.18) = 22.52 F(18.18) = 6.195	Fig. legend
1B AUC	Two-way ANOVA	8-9 per goup	mice from 4 groups	mean +/- SM	GENOTYPE TREATMENT INTERACTION	p = 0.8751 p < 0.0001 p = 0.7743	F(1.30) = 0.02513 F(1.30) = 20.24 F(1.30) = 0.08371	Fig. legend
1C Kinetics	Two-way RM ANOVA	9 per goup	mice from 4 groups	mean +/- SM	TREATMENT TIME INTERACTION	p < 0.0001 p < 0.0001 p < 0.0001	F(3.32) = 40.41 F(6.192) = 129.9 F(18.192) = 17.84	Fig. legend
1C AUC	Two-way ANOVA	9 per group	mice from 4 groups	mean +/- SM	GENOTYPE TREATMENT INTERACTION	p = 0.0173 p < 0.0001 p = 0.5807	F(1.32) = 6.298 F(1.32) = 60.03 F(1.32) = 0.3114	Fig. legend
1D Kinetics	Two-way RM ANOVA	10 per group	mice from 4 groups	mean +/- SM	TREATMENT TIME INTERACTION	p < 0.0001 p < 0.0001 p < 0.0001	F(3.36) = 44.89 F(6.216) = 50.96 F(18.216) = 10.07	Fig. legend
1D AUC	Two-way ANOVA	10 per group	mice from 4 groups	mean +/- SM	SPADIN RILUZOLE INTERACTION	p < 0.0001 p < 0.0001 p = 0.014	F(1.36) = 31.43 F(1.36) = 30.44 F(1.36) = 6.677	Fig. legend

2B	Two-way RM ANOVA	5-9 per group	mice from 4 groups	mean +/- SM	TREATMENT TIME INTERACTION	p < 0.0001 p < 0.0001 p < 0.0001	F(3.3) = 109.1 F(4.12) = 31.75 F(12.12) = 15.53	Fig. legend
2C	Two-way RM ANOVA	5-10 per group	mice from 4 groups	mean +/- SM	TREATMENT TIME INTERACTION	p < 0.0001 p < 0.0001 p < 0.0001	F(3.3) = 22.42 F(4.12) = 8.672 F(12.12) = 5.162	Fig. legend
2D	Two-way RM ANOVA	4-10 per group	mice from 4 groups	mean +/- SM	TREATMENT TIME INTERACTION	p < 0.0001 p = 0.0055 p = 0.0199	F(3.28) = 16.53 F(4.112) = 3.875 F(12.112) = 2.134	Fig. legend
2E	Two-way RM ANOVA	5-10 per group	mice from 4 groups	mean +/- SM	TREATMENT TIME INTERACTION	p = 0.0039 p = 0.0097 p = 0.1051	F(3.3) = 5.518 F(4.12) = 3.497 F(12.12) = 1.584	Fig. legend
2F	Two-way RM ANOVA	5-10 per group	mice from 4 groups	mean +/- SM	TREATMENT TIME INTERACTION	p < 0.0001 p < 0.0001 p < 0.0001	F(3.27) = 166.7 F(4.108) = 26.34 F(12.108) = 12.9	Fig. legend
2G	Two-way RM ANOVA	5-10 per group	mice from 4 groups	mean +/- SM	TREATMENT TIME INTERACTION	p < 0.0001 p < 0.0001 p = 0.0137	F(3.27) = 19 F(4.108) = 6.786 F(12.108) = 2.257	Fig. legend
2H	Two-way RM ANOVA	5-10 per group	mice from 4 groups	mean +/- SM	TREATMENT TIME INTERACTION	p = 0.0021 p = 0.11 p = 0.5637	F(3.28) = 6.292 F(4.112) = 1.932 F(12.112) = 0.8856	Fig. legend
2I	Two-way RM ANOVA	5-10 per group	mice from 4 groups	mean +/- SM	TREATMENT TIME INTERACTION	p < 0.0001 p = 0.0001 p = 0.0126	F(3.29) = 12.05 F(4.116) = 6.267 F(12.116) = 2.271	Fig. legend
3B	Two-way ANOVA	5-10 per group	mice from 4 groups	mean +/- SM	OXALIPLATIN RILUZOLE INTERACTION	p = 0.1239 p = 0.4268 p = 0.4921	F(1.3) = 2.506 F(1.3) = 0.649 F(1.3) = 0.4837	Fig. legend
3C	Two-way ANOVA	6 per group	mice from 4 groups	mean +/- SM	OXALIPLATIN RILUZOLE INTERACTION	p < 0.0001 p = 0.5359 p = 0.5451	F(1.2) = 24.01 F(1.2) = 0.3968 F(1.2) = 0.379	Fig. legend

3D	Two-way ANOVA	5-10 per group	mice from 4 groups	mean +/- SM	OXALIPLATIN RILUZOLE INTERACTION	p = 0.106 p = 0.0415 p = 0.0114	F(1.3) = 2.778 F(1.3) = 4.539 F(1.3) = 7.269	Fig. legend
3E	Two-way ANOVA	6 per group	mice from 4 groups	mean +/- SM	OXALIPLATIN RILUZOLE INTERACTION	p < 0.0001 p = 0.0968 p = 0.5335	F(1.2) = 53.1 F(1.2) = 3.036 F(1.2) = 0.4015	Fig. legend
3F	Two-way ANOVA	5-10 per group	mice from 4 groups	mean +/- SM	OXALIPLATIN RILUZOLE INTERACTION	p = 0.0006 p = 0.1218 p = 0.0429	F(1.3) = 14.5 F(1.3) = 2.536 F(1.3) = 4.471	Fig. legend
3G	Two-way ANOVA	5-10 per group	mice from 4 groups	mean +/- SM	OXALIPLATIN RILUZOLE INTERACTION	p < 0.0001 p = 0.3978 p = 0.8986	F(1.24) = 27.49 F(1.24) = 0.7412 F(1.24) = 0.0167	Fig. legend
4B	Two-way ANOVA	5-10 per group	mice from 4 groups	mean +/- SM	OXALIPLATIN RILUZOLE INTERACTION	p = 0.2091 p = 0.553 p = 0.003	F(1.27) = 1.655 F(1.27) = 4.011 F(1.27) = 10.61	Fig. legend
4C	Two-way ANOVA	5-10 per group	mice from 4 groups	mean +/- SM	OXALIPLATIN RILUZOLE INTERACTION	p < 0.0001 p = 0.1599 p = 0.021	F(1.28) = 24.92 F(1.28) = 2.085 F(1.28) = 11.48	Fig. legend
4D	Two-way ANOVA	5-10 per group	mice from 4 groups	mean +/- SM	OXALIPLATIN RILUZOLE INTERACTION	p = 0.0008 p = 0.5789 p = 0.2766	F(1.3) = 13.75 F(1.3) = 0.3148 F(1.3) = 1.228	Fig. legend
4E	Two-way ANOVA	10, 5, 10, 9	mice from 4 groups	mean +/- SM	OXALIPLATIN RILUZOLE INTERACTION	p < 0.0001 p = 0.3997 p = 0.6522	F(1.3) = 32.31 F(1.3) = 0.73 F(1.3) = 0.2073	Fig. legend
5A	Two-way ANOVA	12-14 per group	mice from 4 groups	mean +/- SM	OXALIPLATIN RILUZOLE INTERACTION	p < 0.0001 p = 0.0125 p = 0.0004	F(1.49) = 49.04 F(1.49) = 6.723 F(1.49) = 14.55	Fig. legend
5B	Two-way ANOVA	9-14 per group	mice from 4 groups	mean +/- SM	OXALIPLATIN RILUZOLE INTERACTION	p < 0.0001 p = 0.0033 p = 0.0002	F(1.46) = 209.2 F(1.46) = 9.642 F(1.46) = 15.84	Fig. legend

5D	Two-way ANOVA	9-11 per group	mice from 4 groups	mean +/- SM	OXALIPLATIN RILUZOLE INTERACTION	p = 0.0018 p = 0.0446 p = 0.0858	F(1.8) = 20.8 F(1.8) = 5.661 F(1.8) = 3.838	Fig. legend
5E	Two-way ANOVA	9-11 per group	mice from 4 groups	mean +/- SM	OXALIPLATIN RILUZOLE INTERACTION	p = 0.0003 p = 0.5053 p = 0.2577	F(1.8) = 37.08 F(1.8) = 0.4863 F(1.8) = 1.485	Fig. legend
6A	Two-way ANOVA	3, 3, 3, 3	cells from 4 groups	mean +/- SM	TREATMENT TIME INTERACTION	p < 0.0001 p < 0.0001 p < 0.0001	F(1.4) = 325.8 F(6.24) = 115.7 F(6.24) = 15.24	Fig legend
6B	Two-way ANOVA	3, 3, 3, 3	cells from 4 groups	mean +/- SM	TREATMENT TIME INTERACTION	p = 0.0007 p < 0.0001 p < 0.0001	F(1.4) = 90 F(6.24) = 136.8 F(6.24) = 33.26	Fig legend
6C	Two-way ANOVA	3, 3, 3, 3	cells from 4 groups	mean +/- SM	TREATMENT TIME INTERACTION	p < 0.0001 p < 0.0001 p < 0.0001	F(2.6) = 479.4 F(6.36) = 118.8 F(12.36) = 35.46	Fig legend
6D	Two-way ANOVA	3, 3, 3, 3	cells from 4 groups	mean +/- SM	TREATMENT TIME INTERACTION	p < 0.0001 p < 0.0001 p < 0.0001	F(1.4) = 994.5 F(6.24) = 235.4 F(6.24) = 95.8	Fig legend
6E	Two-way ANOVA	3, 3, 3, 3	cells from 4 groups	mean +/- SM	OXALIPLATIN RILUZOLE INTERACTION	p < 0.0001 p < 0.0001 p < 0.0001	F(1.8) = 479.4 F(1.8) = 36.49 F(1.8) = 28.95	Fig legend
6F	Two-way ANOVA	3, 3, 3, 3	cells from 4 groups	mean +/- SM	OXALIPLATIN RILUZOLE INTERACTION	p < 0.0001 p < 0.0001 p < 0.0001	F(1.8) = 1160 F(1.8) = 692.3 F(1.8) = 279.5	Fig legend
6G	Two-way ANOVA	3, 3, 3, 3	cells from 4 groups	mean +/- SM	OXALIPLATIN RILUZOLE INTERACTION	p = 0.0201 p = 0.7114 p = 0.8262	F(1.16) = 6.657 F(1.16) = 0.1418 F(1.16) = 0.0498	Fig legend
6H	Two-way ANOVA	3, 3, 3, 3	cells from 4 groups	mean +/- SM	OXALIPLATIN RILUZOLE INTERACTION	p = 0.0029 p = 0.6002 p = 0.5202	F(1.12) = 13.89 F(1.12) = 0.2898 F(1.12) = 0.4389	Fig legend

7B	Two-way RM ANOVA	8 per group	mice from 4 groups	mean +/- SM	TREATMENT TIME INTERACTION	p < 0.0001 p < 0.0001 p < 0.0001	F(3.28) = 119.1 F(4.112) = 29.25 F(12.112) = 6.789	Fig. legend
7C	Two-way RM ANOVA	8 per group	mice from 4 groups	mean +/- SM	TREATMENT TIME INTERACTION	p < 0.0001 p = 0.1282 p < 0.0001	F(3.28) = 25 F(4.112) = 1.829 F(12.112) = 4.8	Fig. legend
7D colon	Two-way ANOVA	8 per group	mice from 4 groups	mean +/- SM	OXALIPLATIN RILUZOLE INTERACTION	p = 0.0008 p = 0.0111 p = 0.274	F(1.28) = 14.26 F(1.28) = 7.406 F(1.28) = 1.245	Fig. legend
7D Duod. + jejunum	Two-way ANOVA	8 per group	mice from 4 groups	mean +/- SM	OXALIPLATIN RILUZOLE INTERACTION	p < 0.0001 p = 0.0014 p = 0.0031	F(1.28) = 97.85 F(1.28) = 12.58 F(1.28) = 10.44	Fig. legend
7D total	Two-way ANOVA	8 per group	mice from 4 groups	mean +/- SM	OXALIPLATIN RILUZOLE INTERACTION	p < 0.0001 p = 0.0019 p = 0.0255	F(1.28) = 55.13 F(1.28) = 11.76 F(1.28) = 7.157	Fig. legend
7E	Two-way ANOVA	8 per group	mice from 4 groups	mean +/- SM	OXALIPLATIN RILUZOLE INTERACTION	p = 0.0016 p = 0.3055 p = 0.729	F(1.28) = 12.14 F(1.28) = 1.09 F(1.28) = 0.1225	Fig. legend
Suppl. data 1	Two-way RM ANOVA	9-10 per group	mice from 6 groups	mean +/- SM	TREATMENT TIME INTERACTION	p < 0.0001 p < 0.0001 p < 0.0001	F(5.52) = 53.24 F(5.26) = 8.992 F(25.26) = 3.943	Fig. legend
Suppl. data 2B	Two-way RM ANOVA	5-10 per group	mice from 4 groups	mean +/- SM	TREATMENT TIME INTERACTION	p = 0.0005 p < 0.0001 p < 0.0001	F(3.23) = 8.532 F(5.115) = 8.026 F(15.115) = 8.178	Fig. legend
Suppl. data 2C	Two-way RM ANOVA	5-10 per group	mice from 4 groups	mean +/- SM	TREATMENT TIME INTERACTION	p = 0.104 p = 0.2225 p = 0.9251	F(3.23) = 2.301 F(5.115) = 1.419 F(15.115) = 0.52	Fig. legend
Suppl. data 3A	Two-way RM ANOVA	8-10 per group	mice from 3 groups	mean +/- SM	TREATMENT TIME INTERACTION	p < 0.0001 p < 0.0001 p < 0.0001	F(2.23) = 50.33 F(4.92) = 28.54 F(8.92) = 6.946	Fig. legend

Suppl. data 3B	One-way ANOVA	8-10 per group	mice from 4 groups	mean +/- SM		p < 0.0001	F = 37.42	Fig. legend
Suppl. data 4	Two-way RM ANOVA	11-12 per group	mice from 4 groups	mean +/- SM	TREATMENT TIME INTERACTION	p = 0.0013 p < 0.0001 p < 0.0001	F(3.42) = 6.258 F(6.252) = 87.68 F(18.252) = 2.992	Fig. legend
Suppl. data 5A	Two-way ANOVA	5-6 per group	mice from 4 groups	mean +/- SM	OXALIPLATIN RILUZOLE INTERACTION	p = 0.6797 p = 0.6733 p = 0.712	F(1.18) = 0.1761 F(1.18) = 0.1837 F(1.18) = 0.1406	Fig. legend
Suppl. data 5B	Two-way ANOVA	5-6 per group	mice from 4 groups	mean +/- SM	OXALIPLATIN RILUZOLE INTERACTION	p = 0.7899 p = 0.2504 p = 0.8893	F(1.18) = 0.07314 F(1.18) = 1.411 F(1.18) = 0.01992	Fig. legend
Suppl. data 5C	Two-way ANOVA	5-6 per group	mice from 4 groups	mean +/- SM	OXALIPLATIN RILUZOLE INTERACTION	p = 0.6797 p = 0.6733 p = 0.712	F(1.18) = 0.1761 F(1.18) = 0.1837 F(1.18) = 0.1406	Fig. legend
Suppl. data 6B	One-way ANOVA	3 per group	mice from 3 groups	mean +/- SM		p = 0.0526	F = 5.007	Fig. legend
Suppl. data 7	Two-way RM ANOVA	6-7 per group	mice from 3 groups	mean +/- SM	TREATMENT TIME INTERACTION	p < 0.0001 p < 0.0001 p < 0.0001	F(2.17) = 118 F(4.68) = 55.69 F(8.68) = 37.15	Fig. legend

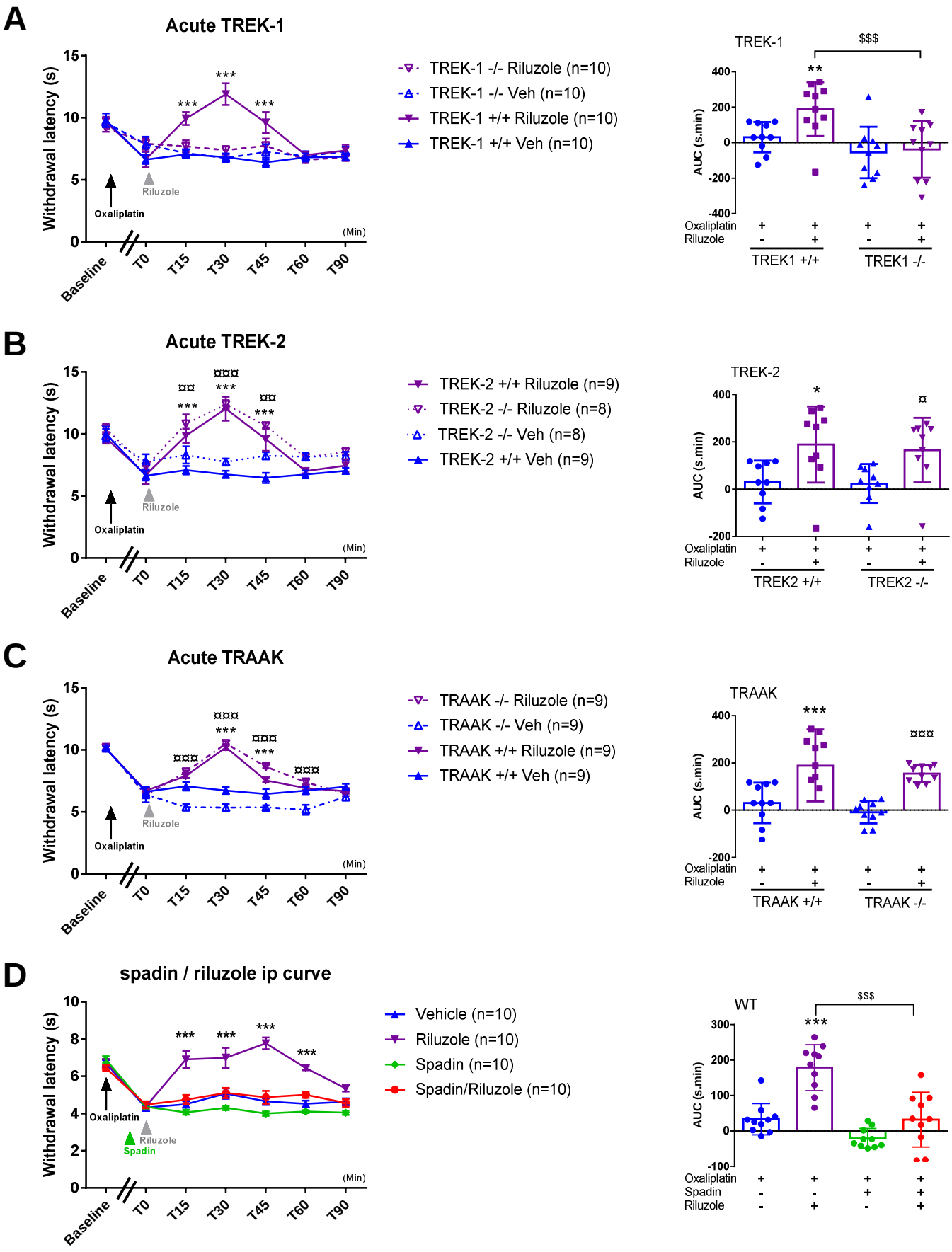
A
Acute TREK-1
Withdrawal latency (s)
Oxaliplatin
Riluzole
(Min)
Baseline
T0
T15
T30
T45
T60
T90
TREK-1 -/- Riluzole (n=10)
TREK-1 -/- Veh (n=10)
TREK-1 +/+ Riluzole (n=10)
TREK-1 +/+ Veh (n=10)
TREK-1
AUC (s.min)
Oxaliplatin
Riluzole
TREK1 +/+
TREK1 -/-
B
Acute TREK-2
TREK-2 +/+ Riluzole (n=9)
TREK-2 -/- Riluzole (n=8)
TREK-2 -/- Veh (n=8)
TREK-2 +/+ Veh (n=9)
TREK-2
TREK2 +/+
TREK2 -/-
C
Acute TRAAK
TRAAK -/- Riluzole (n=9)
TRAAK -/- Veh (n=9)
TRAAK +/+ Riluzole (n=9)
TRAAK +/+ Veh (n=9)
TRAAK
TRAAK +/+
TRAAK -/-
D
spadin / riluzole ip curve
Spadin
Vehicle (n=10)
Riluzole (n=10)
Spadin (n=10)
Spadin/Riluzole (n=10)
WT

Figure 1

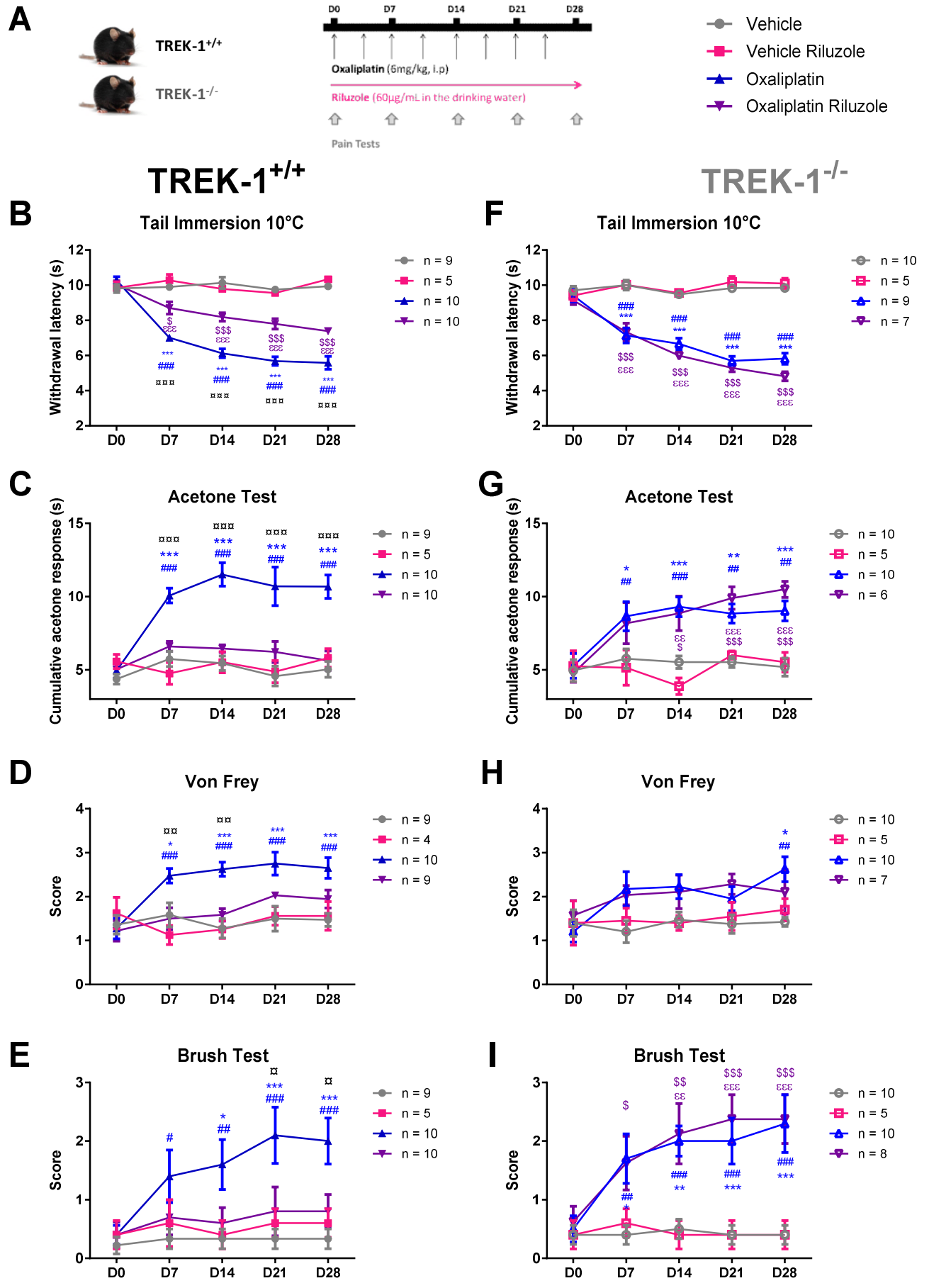
A
TREK-1+/+
TREK-1-/-
D0
D7
D14
D21
D28
Oxaliplatin (6mg/kg, i.p)
Riluzole (60µg/mL in the drinking water)
Pain Tests
Vehicle
Vehicle Riluzole
Oxaliplatin
Oxaliplatin Riluzole
TREK-1+/+
TREK-1-/-
B
Tail Immersion 10°C
Withdrawal latency (s)
n = 9
n = 5
n = 10
n = 10
F
Tail Immersion 10°C
Withdrawal latency (s)
n = 10
n = 5
n = 9
n = 7
C
Acetone Test
Cumulative acetone response (s)
n = 9
n = 5
n = 10
n = 10
G
Acetone Test
Cumulative acetone response (s)
n = 10
n = 5
n = 10
n = 6
D
Von Frey
Score
n = 9
n = 4
n = 10
n = 9
H
Von Frey
Score
n = 10
n = 5
n = 10
n = 7
E
Brush Test
Score
n = 9
n = 5
n = 10
n = 10
I
Brush Test
Score
n = 10
n = 5
n = 10
n = 8

Figure 2

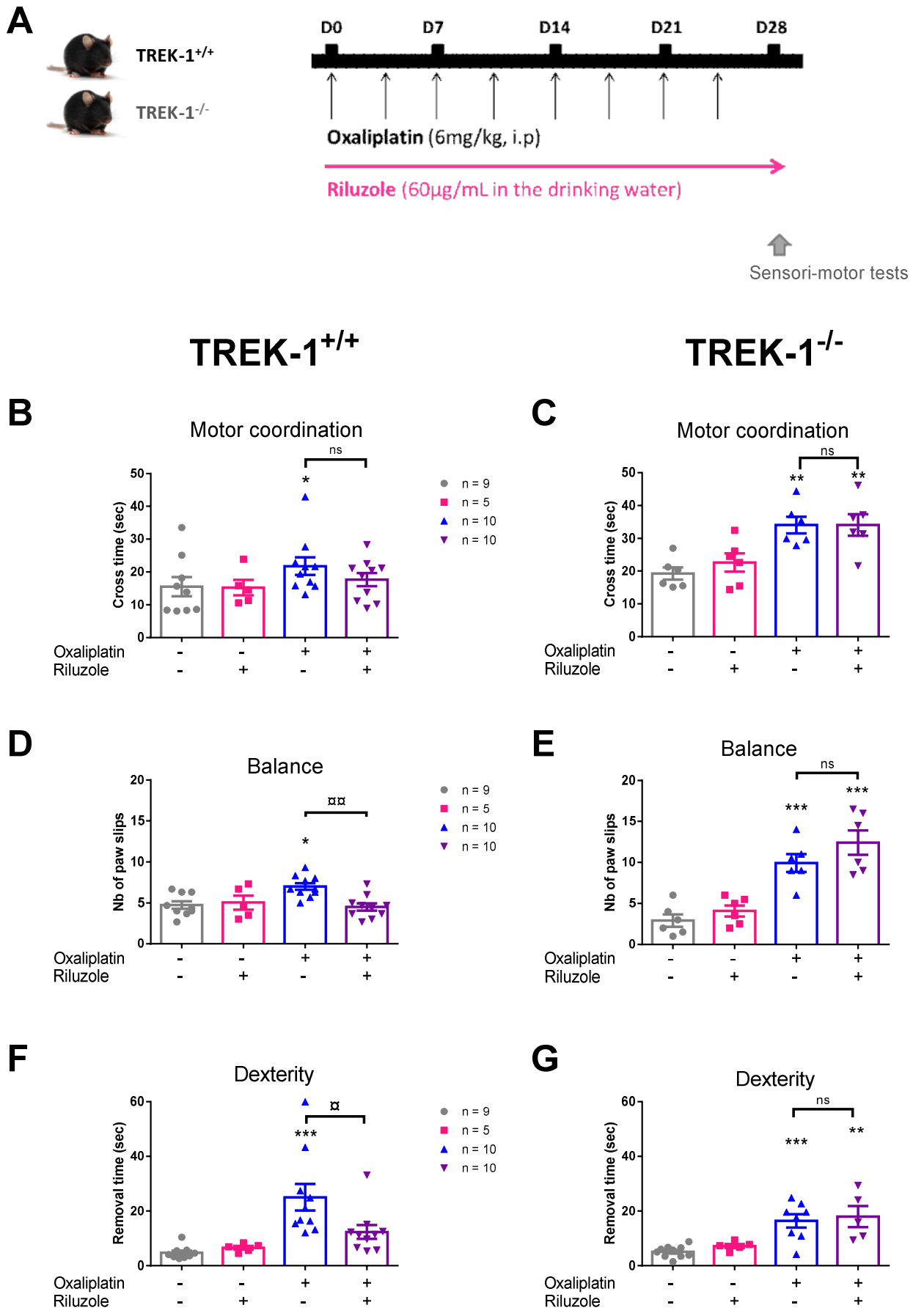
A
TREK-1+/+
TREK-1-/-
D0
D7
D14
D21
D28
Oxaliplatin (6mg/kg, i.p)
Riluzole (60µg/mL in the drinking water)
Sensori-motor tests
TREK-1+/+
TREK-1-/-
B
Motor coordination
Cross time (sec)
C
Motor coordination
Cross time (sec)
D
Balance
Nb of paw slips
E
Balance
Nb of paw slips
F
Dexterity
Removal time (sec)
G
Dexterity
Removal time (sec)
Oxaliplatin
Riluzole
n = 9
n = 5
n = 10
n = 10
n = 6
n = 6
n = 6
n = 6
ns
¤¤
¤

Figure 3

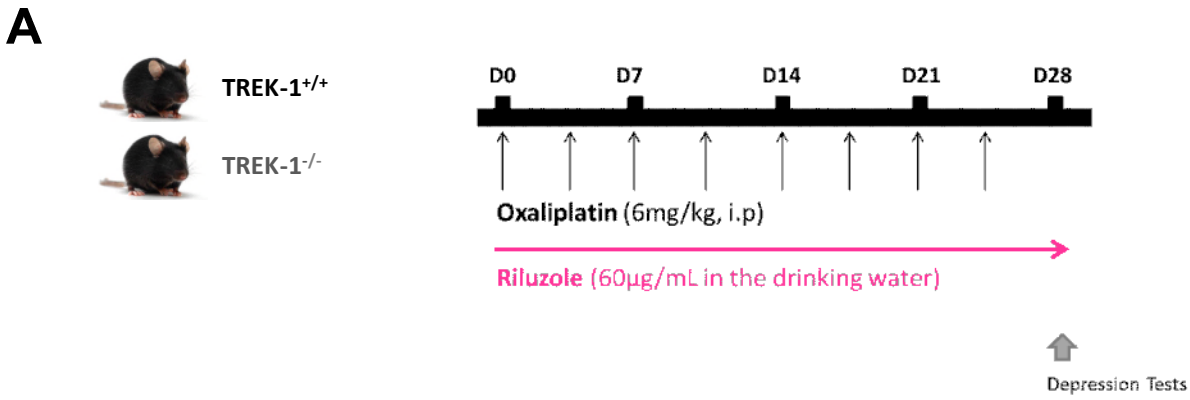
A
TREK-1+/+
TREK-1-/-
D0
D7
D14
D21
D28
Oxaliplatin (6mg/kg, i.p)
Riluzole (60µg/mL in the drinking water)
Depression Tests

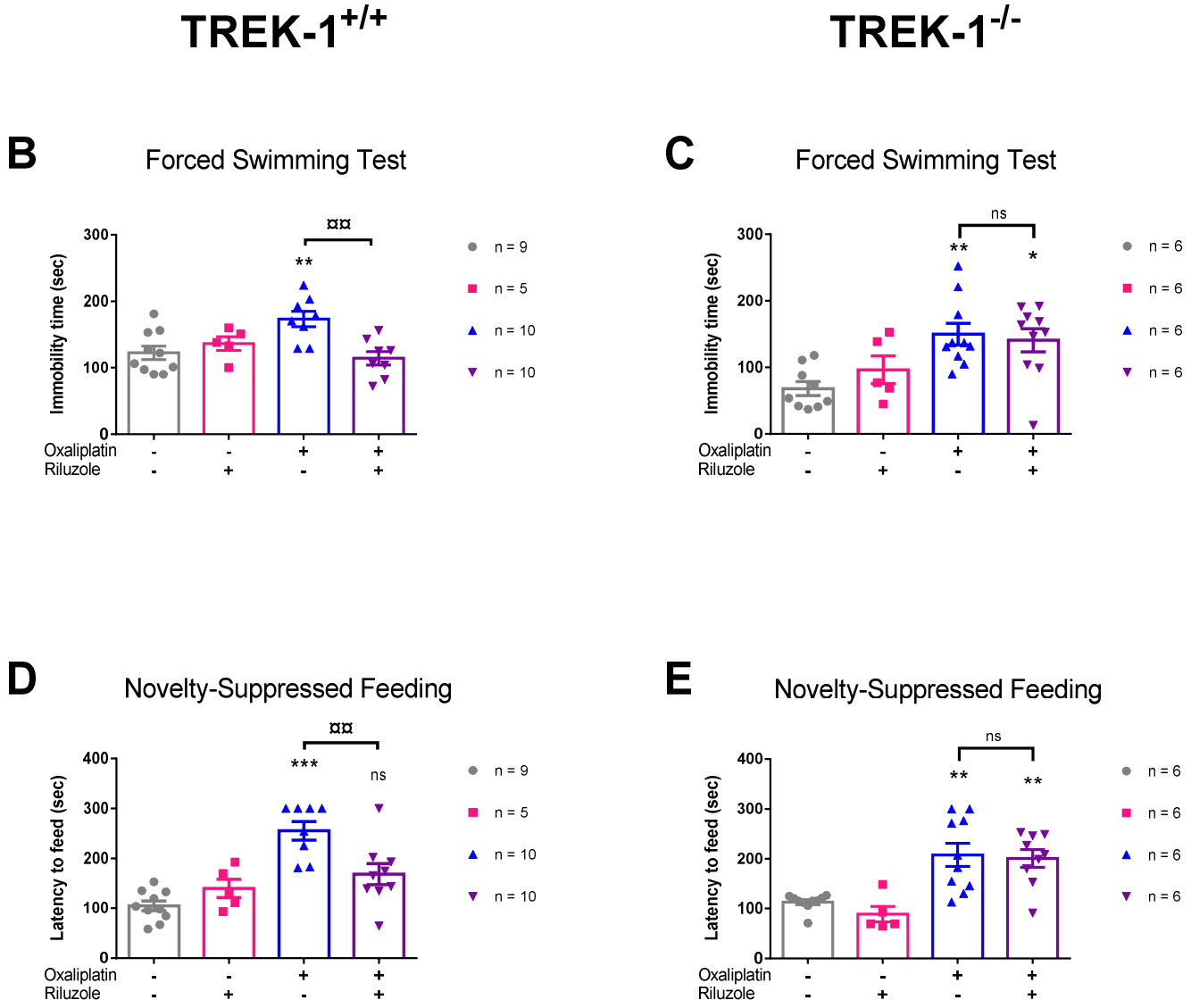
TREK-1+/+
TREK-1-/-
B
Forced Swimming Test
Immobility time (sec)
Oxaliplatin
Riluzole
n = 9
n = 5
n = 10
n = 10
C
Forced Swimming Test
Immobility time (sec)
ns
n = 6
n = 6
n = 6
n = 6
D
Novelty-Suppressed Feeding
Latency to feed (sec)
n = 9
n = 5
n = 10
n = 10
E
Novelty-Suppressed Feeding
Latency to feed (sec)
ns
n = 6
n = 6
n = 6
n = 6

Figure 4

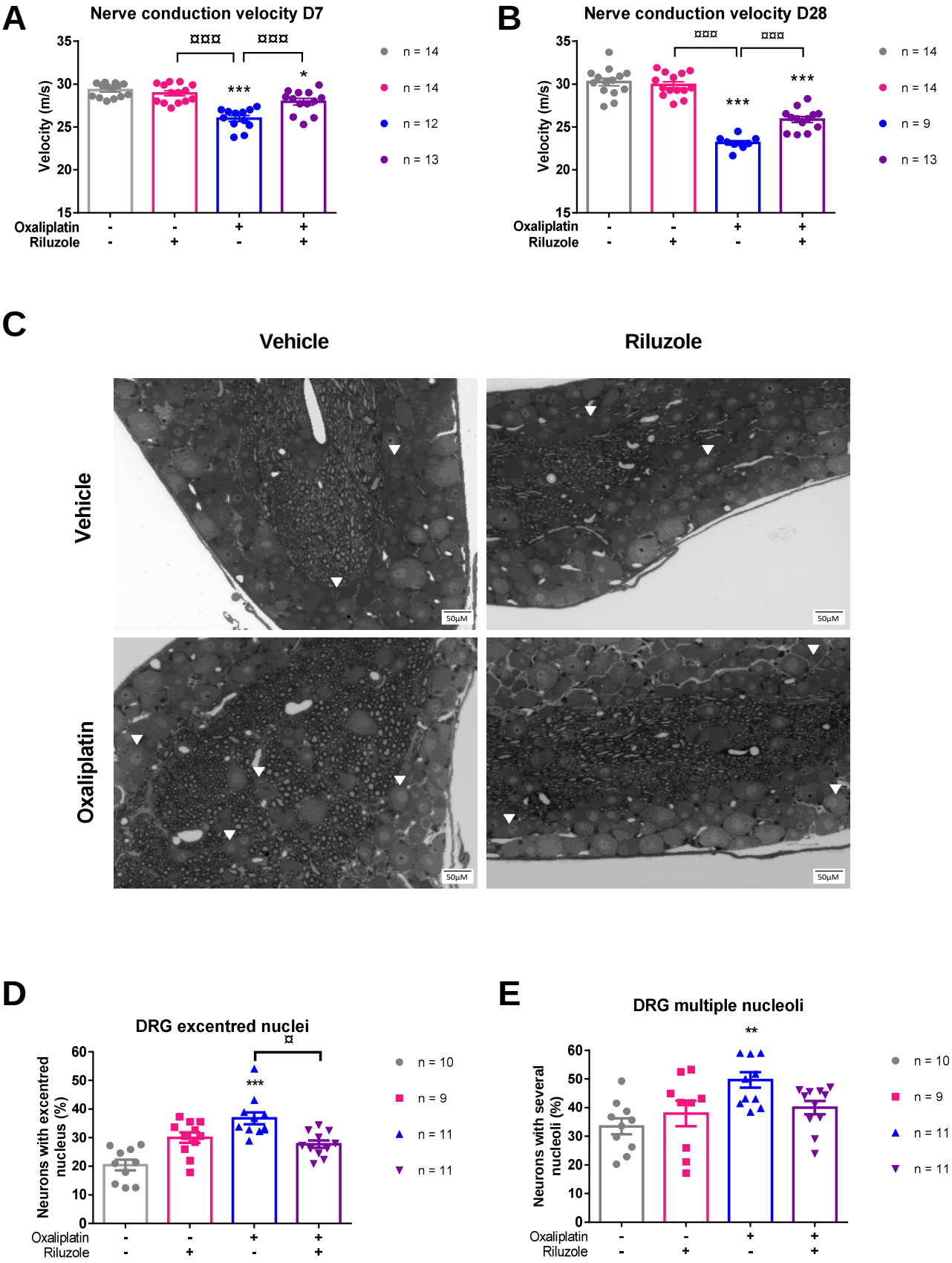
A
Nerve conduction velocity D7
Velocity (m/s)
¤¤¤
¤¤¤
***
*
n = 14
n = 14
n = 12
n = 13
Oxaliplatin
Riluzole
B
Nerve conduction velocity D28
Velocity (m/s)
¤¤¤
¤¤¤
***
***
n = 14
n = 14
n = 9
n = 13
Oxaliplatin
Riluzole
C
Vehicle
Riluzole
Vehicle
Oxaliplatin
50µM
D
DRG excentred nuclei
Neurons with excentred nucleus (%)
¤
***
n = 10
n = 9
n = 11
n = 11
Oxaliplatin
Riluzole
E
DRG multiple nucleoli
Neurons with several nucleoli (%)
**
n = 10
n = 9
n = 11
n = 11
Oxaliplatin
Riluzole

Figure 5

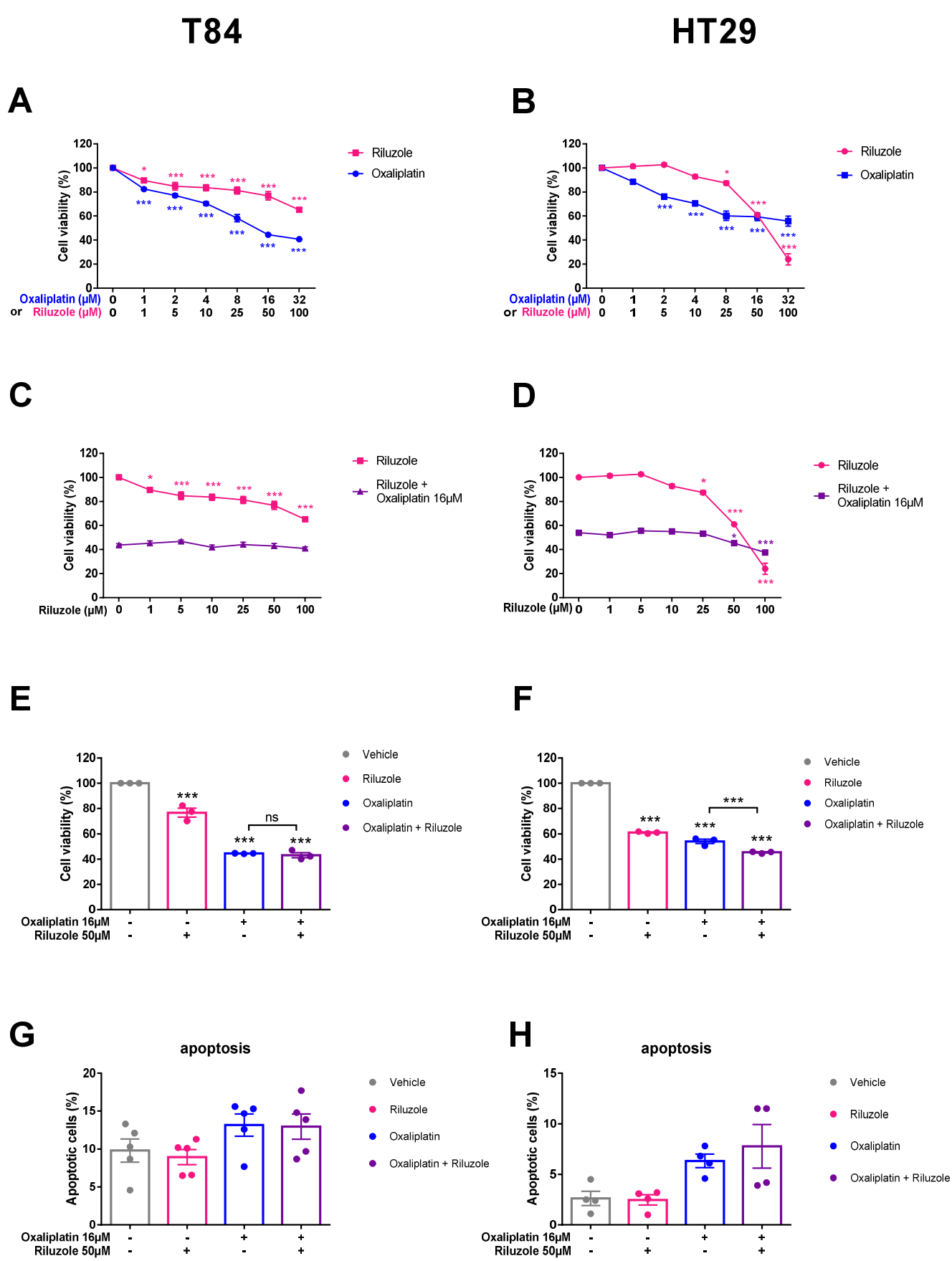
T84
HT29
A
B
C
D
E
F
G
H
Cell viability (%)
Oxaliplatin (μM)
or Riluzole (μM)
Riluzole
Oxaliplatin
Riluzole + Oxaliplatin 16μM
Vehicle
Oxaliplatin + Riluzole
ns
apoptosis
Apoptotic cells (%)
Oxaliplatin 16μM
Riluzole 50μM

Figure 6

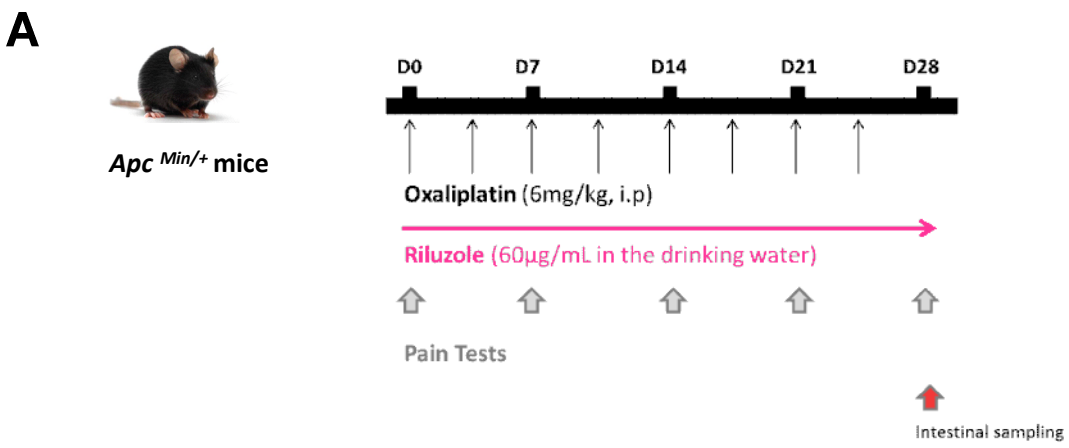
A
Apc Min/+ mice
D0
D7
D14
D21
D28
Oxaliplatin (6mg/kg, i.p)
Riluzole (60µg/mL in the drinking water)
Pain Tests
Intestinal sampling

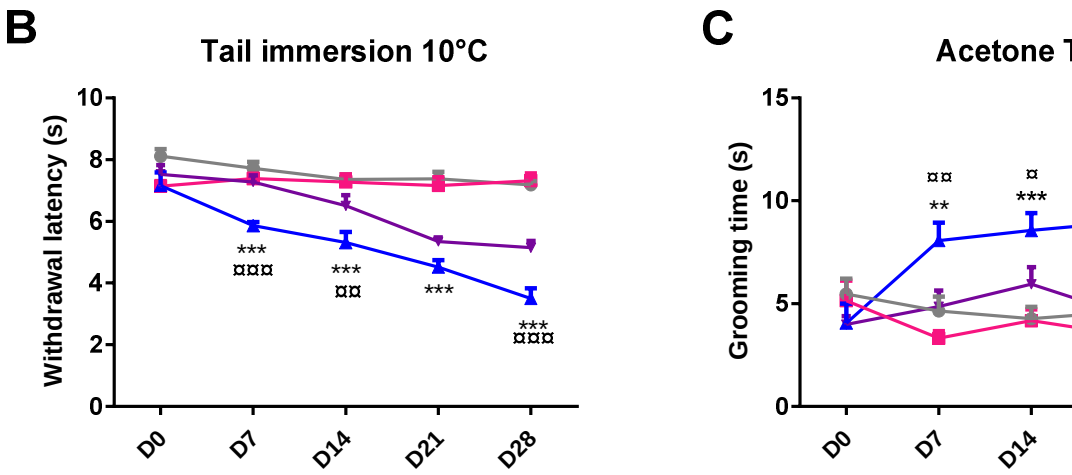
B
Tail immersion 10°C
Withdrawal latency (s)
C
Acetone Test
Grooming time (s)
D0
D7
D14
D21
D28

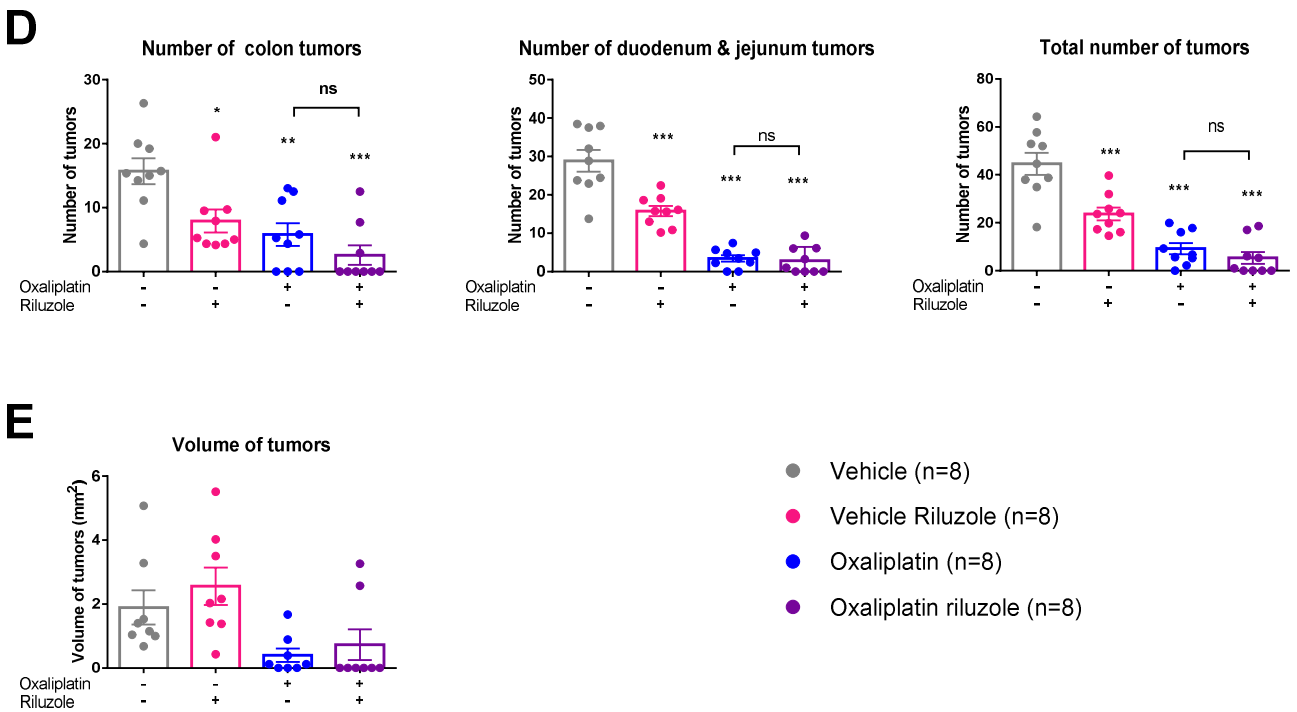
D
Number of colon tumors
Number of duodenum & jejunum tumors
Total number of tumors
Number of tumors
ns
Oxaliplatin
Riluzole

E
Volume of tumors
Volume of tumors (mm²)
Oxaliplatin
Riluzole
Vehicle (n=8)
Vehicle Riluzole (n=8)
Oxaliplatin (n=8)
Oxaliplatin riluzole (n=8)

Figure 7